

X-612-64-240

TM X-55092

N 64 33565

FACILITY FORM 801

(ACCESSION NUMBER)

(PAGES)

(NASA CR OR TMX OR AD NUMBER)

(THRU)

(CODE)

(CATEGORY)

PROPAGATION OF HYDROMAGNETIC WAVES IN THE MAGNETOSPHERE

BY
MASAHISA SUGIURA

AUGUST 1964



GODDARD SPACE FLIGHT CENTER

GREENBELT, MARYLAND

Presented at the Symposium on Ultra Low Frequency Electromagnetic Fields
(from 30 c/s to 0.001 c/s), Boulder, Colorado, August 17-20, 1964.

OTS PRICE

XEROX

MICROFILM

\$ 3.00 FS
\$ 0.25 d/c

PROPAGATION OF HYDROMAGNETIC WAVES IN THE MAGNETOSPHERE

Masahisa Sugiura

NASA - Goddard Space Flight Center

Greenbelt, Maryland

Prepared for presentation at the Symposium on Ultra Low Frequency
Electromagnetic Fields (from 30 c/s to 0.001 c/s), Boulder, Colorado,
August 17-20, 1964

Table of Contents

Abstract

1.	Introduction	1
2.	Propagation of hydromagnetic waves	3
2.1.	The dispersion relation.	3
2.2.	The wave-normal surface.	5
2.3.	Plasma parameter space	8
2.4.	The Clemmow-Mullaly-Allis diagram.	9
2.5.	A model magnetosphere	12
2.6.	The CMA diagram for ULF and VLF waves in the magnetosphere	14
2.7.	Polarization reversal.	16
2.8.	The lower hybrid resonance	20
3.	Ray theory	24
3.1.	Introduction	24
3.2.	The equation of motion of a ray.	24
3.3.	Fermat's principle	27
3.4.	A ray theory for modes with isotropic phase velocity	31
3.5.	Axially symmetric case: <u>allowed</u> and <u>forbidden</u> <u>regions</u> for a ray.	32
3.6.	A further remark on ray tracing in the equatorial plane	35
3.7.	Hydromagnetic rays in the magnetosphere: axially symmetric case	37
3.8.	Hydromagnetic rays in the distorted magnetosphere: axially asymmetric case.	39
4.	Conclusions	44
	Acknowledgements	46
	References	

ABSTRACT

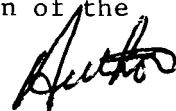
33565 OVER

Characteristics of waves in a two-component cold plasma are reviewed. Using the Clemmow-Mullaly-Allis diagram, the topological types of the wave-normal surfaces are shown. A consistent system of labeling the modes, initially given by Allis, is explained. Reversal in the polarization in the electric field is examined, and all the modes in which the reversal occurs are specified. There is no polarization reversal in ULF to VLF waves in the magnetosphere. The lower hybrid resonance frequency in the magnetosphere is discussed.

The equations of motion for an electromagnetic ray are derived. Defining the action for the ray in analogy with that for a particle in classical mechanics, the principle of least action is proved. It is shown that if the dispersion relation is homogeneous in the wave vector and the frequency, the principle of least action implies the principle of least time, i.e., Fermat's principle. When the principle of least time holds, as is the case with Alfvén compressional waves, the trajectory of a ray can be determined from a variational equation, from which the problem can be formulated in Hamiltonian form. For the axially symmetric case, the generalized momentum conjugate to the azimuthal coordinate is a constant of motion. Using this relation, "allowed" and "forbidden" regions are defined, when a set of initial conditions for the ray is given. This method is applied to a model magnetosphere with a dipole magnetic field. It is shown that the accessibility of hydromagnetic rays originating from the boundary of the magnetosphere to the earth is greatly limited. For a

33565

distorted magnetosphere the canonical equations for a hydromagnetic ray are integrated by a numerical method. Typical trajectories in the equatorial plane are shown, and the effects of the deformation of the dipole field on the ray trajectories are discussed.

A handwritten signature in black ink, appearing to be 'A. C. ...', located to the right of the main text block.

1. Introduction

Hydromagnetic waves can be derived by a low-frequency approximation in a general scheme of treating plasma waves. For a complete understanding of the characteristics of hydromagnetic waves it is desirable to review plasma waves in general for the entire range of frequency and for all possible values of plasma parameters.

Clemmow and Mullaly (1954) presented a comprehensive study of the dependence of the phase refractive index n , derived by the Appleton-Hartree approximation, on the angle θ which the direction of phase propagation makes with that of the magnetic field. These authors developed a systematic method of investigating the topological genera of the (n, θ) surface. Allis (1959), and Allis, Buchsbaum, and Bers (1963) modified the scheme by using the wave-normal surface which is obtained by inverting the (n, θ) surface about the origin. Stix (1962) has given an excellent summary of the wave-normal surface topology for waves in a cold plasma. In Sections 2.1 to 2.9 we will follow Stix's representation.

Stix (1962) called a diagram showing topological genera of the wave-normal surfaces for various regions in plasma parameter space the "Clemmow-Mullaly-Allis diagram", or, in short, the "CMA diagram". The CMA diagram for an idealized two-component cold plasma is presented in Section 2.4, and the characteristics of modes for different regions in plasma parameter space are reviewed. The labeling of modes by the sense of polarization, i.e., "right-handed" or "left-handed", for the propagation parallel to the magnetic field, or by "ordinary" or "extraordinary" mode according as the refractive index for the propagation perpendicular to the magnetic field is

independent or dependent on the magnetic field is explained using the CMA diagram.

In Section 2.6 the wave-normal surface topology in those regions in the CMA diagram that are relevant to ULF and VLF waves in the magnetosphere is studied.

Reversal of the polarization in the electric field that may occur for θ not equal to 0 is examined in detail (Section 2.7), and the lower hybrid resonance frequency in the magnetosphere is presented (Section 2.8).

In Sections 3.1 to 3.3 geometrical electromagnetics, or ray theory, is formulated, and in Sections 3.4 to 3.8 the theory is applied to the propagation of hydromagnetic waves in the magnetosphere.

Analogy between the Hamiltonian form of classical mechanics and geometrical electromagnetics is demonstrated (Sections 3.2, 3.3, 3.4), and validity of Fermat's principle in geometrical electromagnetics is examined (Section 3.3). The action is defined for a ray, and the principle of least action is established. It is then shown that if the dispersion relation is homogeneous in \mathcal{K} and ω , the principle of least action implies the principle of least time, i.e., Fermat's principle. This is the same result as that obtained by Weinberg (1962) by the eikonal theory.

By formulating the ray theory in Hamiltonian form it is shown (Section 3.5) that when the magnetic field and the plasma are axially symmetric, and when the wave-normal surface is spherical, the generalized momentum conjugate to the azimuthal coordinate is a constant of motion. Applying this result to the propagation of hydromagnetic waves in a dipole

model magnetosphere (Section 3.5), we will define, for a set of initial conditions of a ray, "forbidden" and "allowed" regions for the ray in the same manner as Störmer (1953) did for a charged particle moving in a dipole magnetic field. It will be shown that because of the Alfvén velocity maximum at an altitude of several thousand kilometers above ground the accessibility of hydromagnetic rays generated in the outer regions of the magnetosphere to the immediate vicinity of the earth is very limited.

When the magnetic field is not axially symmetric, the canonical equations must be integrated. In Section 3.8 we will present examples of hydromagnetic ray trajectories computed by numerical method for a model magnetosphere that takes into account the distortion of the dipole field by solar wind. Trajectories in the equatorial plane alone are presented in Section 3.8; more detailed discussions will be given in a separate paper.

2. Propagation of hydromagnetic waves

2.1. The dispersion relation

The dispersion relation for waves in a cold plasma in a uniform magnetic field has been given by Åström (1950), Sitenko and Stepanov (1957) and Allis (1959). Here we only outline the derivation of the dispersion relation; for the details, see, e.g., Stix (1962).

We assume that in the unperturbed state the magnetic field \vec{B}_0 and the plasma are static and uniform, and we take \vec{B}_0 and the quantities characterizing the plasma to be zero-order quantities. The perturbation \vec{B} in the magnetic field, the electric field \vec{E} , the current and the particle velocities

are considered to be first-order variables, and the relevant equations are all linearized by ignoring second- and higher-order terms. The first-order variables are assumed to change as $\exp i (\vec{k} \cdot \vec{r} - \omega t)$.

Considering the displacement current to be the sum of that in vacuum and the plasma current, and by Fourier analysis the electric displacement \vec{D} can be expressed in the form

$$\vec{D} = \vec{K} \cdot \vec{E}$$

thus defining the dielectric tensor \vec{K} .

The expression for \vec{D} and Maxwell's equations yield the following dispersion relation in terms of the refractive index n :

$$A n^4 - B n^2 + C = 0 \quad (1)$$

where

$$A = S \sin^2 \theta + P \cos^2 \theta$$

$$B = RL \sin^2 \theta + PS (1 + \cos^2 \theta)$$

$$C = PRL$$

$$S = \frac{1}{2} (R + L)$$

$$R = 1 - \sum_{\vec{k}} (\Pi_{\vec{k}}^2 / \omega^2) / (1 + \epsilon_{\vec{k}} \Omega_{\vec{k}} / \omega)$$

$$L = 1 - \sum_{\vec{k}} (\Pi_{\vec{k}}^2 / \omega^2) / (1 - \epsilon_{\vec{k}} \Omega_{\vec{k}} / \omega)$$

$$P = 1 - \sum_{\vec{k}} \Pi_{\vec{k}}^2 / \omega^2$$

$$\Pi_{\vec{k}}^2 = 4 \pi n_{\vec{k}} q_{\vec{k}}^2 / m_{\vec{k}}$$

$$\Omega_{\vec{k}} = |q_{\vec{k}}| B_0 / (m_{\vec{k}} c)$$

$$\epsilon_{\vec{k}} = q_{\vec{k}} / |q_{\vec{k}}|$$

(2)

Here the subscript k refers to the particle of type k whose mass and charge are m_k and q_k , respectively, and c is the velocity of light; π_k and Ω_k are the plasma frequency and the cyclotron frequency for the k -th constituent; ϵ_k merely specifies the sign of the charge.

2.2. The wave-normal surface

When all the plasma parameters and the frequency ω are specified, n is a function of θ , the angle between the static magnetic field \vec{B}_0 and the wave vector \vec{k} . Denoting the unit vector in the direction of \vec{k} by \vec{k} , \vec{k}/n gives the phase velocity, measured in units of c , in the direction of phase propagation.

We define the wave-normal surface by revolving about the direction of the magnetic field \vec{B}_0 the locus of the tip of the vector \vec{k}/n when θ is changed from 0 to π ; since the magnetic field and the plasma are assumed to be uniform, at each point in space the wave-normal surface is axially symmetric about the direction of the magnetic field. Thus the topological nature of the wave-normal surface is determined by the dependence of n on θ .

From the dependence of the coefficients A and B in (1) on θ as indicated in (2) it is obvious that the wave-normal surface is symmetric with respect to the plane through the origin and normal to the magnetic field; namely, $n(\theta) = n(\pi - \theta)$.

The solutions of (1) are

$$n^2 = (B \pm F)/(2A) \quad (3)$$

where

$$F^2 = (RL - PS)^2 \sin^4\theta + P^2 (R - L)^2 \cos^2\theta$$

There are two branches in n^2 , and for real values of θ , n is either pure real or pure imaginary.

The solutions for n^2 for propagation at $\theta = 0$ (parallel to the magnetic field) and $\theta = \frac{1}{2}\pi$ (perpendicular to the magnetic field) reduce to the following simple expressions.

For $\theta = 0$,

$$n^2 = R \tag{4}$$

$$n^2 = L \tag{5}$$

and for $\theta = \frac{1}{2}\pi$,

$$n^2 = RL/S \tag{6}$$

$$n^2 = P \tag{7}$$

It can be shown that for $\theta = 0$, the polarization of the electric field for the branch with $n^2 = R$ is circular and right-handed and that for the branch $n^2 = L$ also circular but left-handed.

For $\theta = \frac{1}{2}\pi$, the phase velocity for the branch with n^2 given by (6) depends on the magnetic field, whereas that for the branch represented by (7) is independent of the magnetic field.

These characteristics at $\theta = 0$ and $\theta = \frac{1}{2}\pi$ will be used later for labeling the modes.

To study the shape of the wave-normal surface it is important to know where n^2 becomes 0 or infinity. For instance, if n^2 crosses 0 from positive to negative, then n becomes imaginary and hence the wave becomes evanescent.

Equation (1) shows that $n^2 = 0$ is a solution only if $C = 0$, namely, if

$$P = 0, \text{ or } R = 0, \text{ or } L = 0. \quad (8)$$

Then the phase velocity is infinite.

The other case, $n^2 = \infty$ occurs when $A = 0$; from (2) we see that this happens when θ satisfies the relation

$$\tan^2 \theta = - P/S \quad (9)$$

Thus, if P and S are of opposite sign, then at θ satisfying (9) and also at $\pi - \theta$, n^2 is infinite and the phase velocity is zero. When this happens, n^2 is zero at no other real θ . At $\theta = 0$, n^2 is ∞ when $S = \pm \infty$, and at $\theta = \frac{1}{2}\pi$, n^2 is ∞ when $S = 0$.

A circumstance in which $n^2 = 0$ is called a cutoff and that in which $n^2 = \infty$ a resonance (Allis, 1959). Allis calls the resonances at $\theta = 0$ and $\theta = \frac{1}{2}\pi$ the principal resonances.

From (4) and (5) we see that at $\theta = 0$, $n^2 = \pm \infty$, when $R = \pm \infty$, or $L = \pm \infty$. The definitions in (2) show that the case $R = \pm \infty$ corresponds to electron cyclotron resonance and the case $L = \pm \infty$ to ion cyclotron resonance. Indeed, the polarization of the electric field in each case can be shown to be in the same direction as that of gyration of the respective particle.

The resonance at $\theta = \frac{1}{2}\pi$, corresponding to $S = 0$, is called the hybrid resonance; there are two branches in the solution to $S = 0$, and according to the frequency, the two resonances are called the upper and

the lower hybrid resonances. The lower hybrid resonance will be discussed in Section 2.8.

In the limit $\theta \rightarrow 0$ and $P \rightarrow 0$, a resonance may or may not result, depending upon the path of approach to this double limit (Stix, 1962).

The topological characteristics of the wave-normal surfaces can be classified into three categories. If n^2 is positive for all real values of θ , the wave-normal surface is topologically equivalent to a sphere.

As we have seen, if P and S are of opposite sign, there is a resonance at θ_{res} satisfying (9). In this case, if n^2 is positive for $0 \leq \theta \leq \theta_{res}$, and for $\pi - \theta_{res} \leq \theta \leq \pi$ and negative for $\theta_{res} < \theta < \pi - \theta_{res}$, the wave-normal surface is equivalent to a dumbbell-shaped lemniscoid. If the sign of n^2 in these regions is reversed, the wave-normal surface is equivalent to a wheel-shaped lemniscoid.

2.3. Plasma parameter space

To determine the wave-normal surfaces for the two branches of n^2 certain parameters of the plasma must be specified. Equations (1) and (2) indicate that the wave-normal surfaces are uniquely determined when the ratios Π_k/ω and Ω_k/ω (and ϵ_k) are specified for all k . Thus, if we imagine $2k$ -dimensional space with $2k$ mutually orthogonal axes representing Π_k/ω and Ω_k/ω , the wave-normal surfaces for the two branches of n^2 can be assigned to every point in this plasma parameter space. However, if we specify fixed parameters, such as ratios of number densities of different types of particles, and mass ratios, the minimum number of coordinate axes required is reduced.

To be specific in our representation we now limit ourselves to a neutral cold plasma consisting of electrons and hydrogen ions. We denote the plasma frequencies and the cyclotron frequencies for electrons and ions by affixing subscript e or i to Π and Ω .

The quantities R, L, and P defined in (2) are then reduced to much simpler expressions:

$$R = 1 - \alpha / [(1 + \Omega_i/\omega)(1 - \Omega_e/\omega)] \quad (10)$$

$$L = 1 - \alpha / [(1 - \Omega_i/\omega)(1 + \Omega_e/\omega)] \quad (11)$$

$$P = 1 - \alpha \quad (12)$$

where

$$\alpha = (\Pi_e^2 + \Pi_i^2) / \omega^2 \quad (13)$$

Since $\Omega_e/\Omega_i = m_i/m_e \equiv \mu$, is a fixed parameter, we see that two-dimensional parameter space, i.e., a plane, suffices for our purpose. Following Allis (1959) and Stix (1962) we take Ω_e^2/ω^2 as ordinate and α as abscissa; we are only concerned with the quadrant bounded by the positive axes.

2.4. The Clemmow-Mullaly-Allis diagram

We now divide this plasma parameter plane into bounded areas by curves representing the principal resonances and cutoffs. To make the bounding curves reasonably separated from each other it is helpful to

take the ion-to-electron mass ratio μ to be smaller than its actual value. Following Allis and Stix, we take μ to be 4 for our illustrative purpose.

By examining the wave-normal surfaces in the manner described in the preceding Section it can be shown that the topological type of each of the wave-normal surfaces for the two branches remains the same throughout each of the bounded areas.

The CMA diagram constructed in this way is shown in Figure 1. In each of the bounded areas the topological types of the wave-normal surfaces for the two branches are indicated. Wherever only one wave-normal surface is drawn, the mode corresponding to the other branch is evanescent, and in the area to the right of the curve $L = 0$ and below the horizontal line $R = \infty$ both branches are evanescent.

The curve for $RL - PS = 0$ is drawn in with broken lines. This curve represents neither cutoff nor resonance, but it proves to be useful in labeling the modes.

As we have seen in Section 2.2 the polarization in the electric field is either right-handed or left-handed at $\theta = 0$. The wave-normal surfaces in Figure 1 are labeled R or L on top of each sketch according as the polarization at $\theta = 0$ is right-handed or left-handed, respectively.

For the propagation across the magnetic field, i.e., $\theta = \frac{1}{2}\pi$, we found that n^2 for one of the two branches depends on the magnetic field and that n^2 for the other branch is independent of the magnetic field. Allis (1959) termed the mode with n^2 dependent on the magnetic field "extraordinary" mode and the mode with n^2 independent on the magnetic field

"ordinary" mode. We follow Allis' nomenclature, and wherever the propagation in this direction ($\theta = \frac{1}{2}\pi$) is possible, the symbol O or X is attached to the right of each sketch of the wave-normal surface, according as the mode is "ordinary" or "extraordinary".

This system of labeling the modes seems to be most systematic and is recommended for the general use to eliminate confusion that has existed in the past.

As we shall see in Section 2.9, for frequencies much less than the ion cyclotron frequency the wave-normal surface for the mode labeled with R and X in Figure 1 becomes a sphere, that is, n^2 is independent of θ . For this reason Åström (1950) called this mode "ordinary" and the other "extraordinary", and Åström's nomenclature has been used widely in the literature dealing with hydromagnetic waves. However, this labeling is not consistent with Allis' system. Since the spherical wave-normal surface in question is merely an approximation valid only for frequencies well below the ion cyclotron frequency, Allis' system seems to be preferable.

As is evident in Figure 1, a right-handed (or left-handed) mode at $\theta = 0$ may be either an ordinary or extraordinary mode at $\theta = \frac{1}{2}\pi$, and hence labeling the modes with only one label R or L, or O or X is not adequate.

It is also noted that the polarization in the electric field may reverse its direction in some regions in the plasma parameter plane (Stix, 1962). This problem will be discussed in detail in Section 2.7.

The two modes can be distinguished by still another labeling method. The two modes are labeled "fast" or "slow" by comparing the size of the

wave-normal surfaces. There can be no crossing of the wave-normal surfaces for the two branches so that the labeling with "fast" or "slow" mode can be made unambiguously. Wherever only one branch is nonevanescant, it is reasonable to assume that the wave-normal surfaces change continuously in the plasma parameter plane and to label that mode consistently with the naming of the corresponding mode in the neighboring bounded areas where a comparison of two modes is possible.

2.5. A model magnetosphere

In Section 2.6 a CMA diagram for ULF and VLF waves in the magnetosphere will be presented. The model magnetosphere to be used for the CMA diagram and also for all the discussions of hydromagnetic waves in the later Sections is described in this Section.

We approximate the earth's magnetic field by a dipole except in Section 3.8 where the distortion of the dipole field due to solar wind is taken into account.

The electron density distribution in the magnetosphere adopted here is based on the recent determination by Liemohn and Scarf (1964) using nose whistlers. Among the electron density distributions which these authors considered to give self-consistent results, we adopt the simplest distribution, namely, the model in which the electron density is inversely proportional to the distance from the earth's center. Their results apply to the region of the magnetosphere approximately from 3 to 5 earth-radii. We assume that this inverse cube law for the electron density holds in regions below and above

these altitudes. To be precise, we assume that the electron density varies as $N_0(a/r)^3$ on the equatorial plane from 15,000 km geocentric distance to the boundary of the magnetosphere which is taken to be at $10a$; here a is the radius of the earth and N_0 is taken to be 1.41×10^4 electrons/cm³ (Liemohn and Scarf, 1964).

For altitudes below the bottom limit of the above distribution (15,000 km geocentric distance) we base our model on that given by Dessler, Francis, and Parker (1960), but to ensure continuity of the electron density we apply smoothing. In so doing the region below 15,000 km was divided into two regions and in each region the electron density was expressed in a power series. At the boundary between the two regions and at 15,000 km geocentric distance, the electron density and its first derivative with respect to radial distance are made continuous. The density was expressed analytically for the convenience for the numerical calculations required later in the ray treatment.

Figure 2 shows the electron density distribution constructed in the manner described above and used throughout this paper. The distribution given in Figure 2 refers to that in the equatorial plane, but we assume that the electron density is a function of radial distance alone.

Figure 3 shows the electron plasma frequency and the electron cyclotron frequency as functions of geocentric distance. The former is assumed to be spherically symmetric, but the latter, of course, varies with latitude.

2.6. The CMA diagram for ULF and VLF waves in the magnetosphere

Having obtained in Section 2.3 the whole view of the CMA diagram for an idealized plasma in which the ion-to-electron mass ratio is taken to be 4, we now ask what regions in the plasma parameter plane are relevant to propagation of ULF and VLF waves in the magnetosphere. We will now take the actual value for the hydrogen-ion-to-electron mass ratio μ .

In Section 2.3 we took α and Ω_e^2/ω^2 as coordinates, but the conditions that are of interest to us now make it more convenient to use π_e/ω as abscissa and Ω_e/ω as ordinate.

A CMA diagram for ULF and VLF with these coordinate axes is shown in Figure 4. The diagram can be used in two ways. If the frequency ω is specified, the change in the plasma parameters with distance from the earth's center (for instance, on the equatorial plane) can be represented by a curve along which the radial distance is marked.

Alternatively, if a position in the magnetosphere is specified, a continuous change in the wave frequency at that position can be represented by a continuous curve in the CMA diagram.

For the sake of convenience we take the former representation. In Figure 4, curves are drawn for frequencies from 0.01 c/sec to 10 kc/sec. Since the plasma parameter variations with radial distance are the same for all frequencies, curves for different frequencies can be obtained from one of them by merely displacing it parallel to a fixed straight line.

Since the magnetic field varies with latitude, the curves drawn in

Figure 4 for the equatorial plane will be changed at higher latitudes, but the changes are only slight because of the logarithmic scale in the diagram, and the general features which are discussed below will not be altered appreciably.

First, we observe that for waves with frequencies below about 1 c/sec, two modes are possible. One has a wave-normal surface topologically equivalent to a sphere; its electric field has right-handed circular polarization at $\theta = 0$, and the mode is "extraordinary" at $\theta = \frac{1}{2}\pi$; this mode is the "fast" mode. The other mode, which is the "slow" mode, has a wave-normal surface topologically equivalent to a dumbbell-shaped lemniscoid, and its electric field has left-handed circular polarization at $\theta = 0$. In the hydromagnetic approximation the former mode corresponds to Alfvén compressional wave and the latter to Alfvén shear wave. It is the latter mode that Alfvén (1942) originally derived by treating plasma as a conducting fluid.

In the frequency range approximately from 1 c/sec to 100 c/sec, ion cyclotron resonance takes place at some altitude, and above this altitude only the fast mode can propagate. (We are concerned here only with altitudes above several hundred kilometers above ground level.)

For each frequency in the range from several tens cycles/sec to several kilocycles/sec, the lower hybrid resonance (at $\theta = \frac{1}{2}\pi$, and $S = 0$) is encountered at a certain altitude, and above that altitude the wave-normal surface is transformed to a dumbbell-shaped lemniscoid; propagation across the magnetic field becomes impossible. The mode

prevailing at frequencies above the lower hybrid resonance frequency is the "whistler" mode.

As we go to still higher frequencies we reach electron cyclotron resonance, and the whistler mode is destroyed. If we cross the cutoff $L = 0$ from right to left in Figure 4, we have one or two modes, according as the frequency is above or below the electron cyclotron resonance. In the latter case the slow mode represents the whistler mode.

2.7. Polarization reversal

In this Section we examine polarization at θ not equal to zero. In Section 2.4 we already mentioned the possibility of reversal of polarization.

Stix (1962) showed that for one of the branches the polarization of the electric field changes direction of rotation at θ satisfying the relation

$$\sin^2\theta = P/S \quad (14)$$

Clearly, for this reversal of polarization to take place at real θ , P and S must be of the same sign and $|P/S| \leq 1$. Even these conditions are both satisfied, the reversal may occur in an evanescent branch. Thus it is worthwhile examining the problem in detail.

From the condition that P and S are of the same sign we can eliminate about one half of the bounded areas in the CMA diagram. By the second condition, namely, that $|P/S| \leq 1$, part of the remaining areas are further eliminated. In Figure 5, areas where polarization reversal cannot occur are shaded; signs of P and S are indicated by a small symbol $+$ or $-$. The

coordinates in Figure 5 are the same as in Figure 1, and the ion-to-electron mass ratio μ is again taken to be 4; this is just for schematical representation, and our discussion in this Section applies to the case in which μ is taken to be the actual ion-to-electron mass ratio. The horizontal line at $\Omega_e^2/\omega^2 = \mu^2$ corresponds to $\Omega_i^2 = \omega^2$, i.e., ion cyclotron resonance. Another horizontal line at $\Omega_e^2/\omega^2 = \mu^2 - \mu + 1$ plays an important role in the following discussions. This comes about from the fact that P - S has the factor $\Omega_e^2/\omega^2 - (\mu^2 - \mu + 1)$ in the numerator. For $\mu > 1$, $\mu^2 - \mu + 1$ is less than μ^2 and is greater than 1. It can be shown that $\mu^2 - \mu + 1$ is the ordinate (Ω_e^2/ω^2) for the intersection of P = 0 and S = 0, and that the curve RL - PS = 0 intersects the Ω_e^2/ω^2 axis at $\mu^2 - \mu + 1$.

From Figure 5 it is already clear that the reversal can never occur in the magnetosphere in waves with frequencies below the ion cyclotron frequency.

Next we examine in which branch the polarization reversal takes place, if it does at all, without limiting ourselves to the conditions of our immediate interest.

By examining the polarization of the electric field it can be shown that if the polarization reversal occurs, then it does so in the branch that comes from the positive sign in (3) when $RL + PS - 2S^2$ is negative, and in the branch from the negative sign in (3) when this quantity is positive.

It is, therefore, instructive to locate the solution to the equation

$$RL + PS - 2S^2 = 0 \quad (15)$$

The left-hand side of (15) can be written as follows:

$$\begin{aligned}
 \text{RL+PS} - 2S^2 = & -\alpha x^2 (\mu^2 - x^2)^{-2} (1 - x^2)^{-2} [x^6 - \{2\mu^2 - (1+\alpha)\mu + 2\} x^4 \\
 & + \{\mu^4 - (1+\alpha)\mu^3 + 3\mu^2 - (1+\alpha)\mu + 1\} x^2 \\
 & - \mu^2 \{(1 - 2\alpha)\mu^2 - (1 - 3\alpha)\mu + 1 - 2\alpha\}] \quad (16)
 \end{aligned}$$

where $x = \Omega_e / \omega$

The expression on the right-hand side of (16) can also be written as

$$\begin{aligned}
 & -\alpha x^2 (\mu^2 - x^2)^{-2} (1 - x^2)^{-2} [(x^2 - \mu^2) \{x^2 - (\mu^2 - \mu + 1)\} (x^2 - 1) \\
 & + \alpha \mu \{(x^2 - \mu^2) (x^2 - 1) + 2\mu(\mu - 1)^2\}]
 \end{aligned}$$

Though the latter expression is convenient to determine α when x^2 is given, we will use (16) to obtain the solution to (15). From (16) we see that $x^2 = 0$ is a solution of (15), which, however, is of no interest to us.

We now examine the solution of the equation that is obtained by equating the content of the square brackets in (16) to zero. Since the equation so obtained is cubic in x^2 , we can determine the number of real roots by examining the discriminant. This method is helpful in locating the solutions.

For $\alpha \gg \mu$ and x^2 not very much greater in order of magnitude than μ , x^2 becomes independent of α , and we have two positive roots:

$$x^2 = \mu^2 (1 - 2/\mu) \quad \text{or} \quad 2\mu$$

thus, giving two positive roots for x

$$x = \mu (1 - 2/\mu)^{\frac{1}{2}} \quad \text{or} \quad (2\mu)^{\frac{1}{2}}$$

Numerically, these are approximately 1835.50 and 60.64, respectively.

There are three positive real roots (x^2 satisfying (15)) for positive α less than 0.175. Between 0.175 and 5.835 there is only one negative real root. For α greater than 5.835 there are two positive real roots and one negative real root. (The numbers quoted are accurate to ± 0.005 .)

The curves representing (15) are schematically shown in Figure 6; the sign for $RL + PS - 2S^2$ is also indicated for areas separated by the curves.

We now combine the results in Figures 5 and 6. In so doing we observe that the intersection of $R = \infty$ and $L = 0$ is at $\alpha = 2(1 - 1/\mu) < 2$. We see that all the unshaded areas in Figure 5 where the polarization reversal can occur are in the regions where $RL + PS - 2S^2$ is negative. Thus the reversal occurs in the branch resulting from the plus sign in (3).

We reach the conclusion that there is no polarization reversal in the nonevanescant modes to the right of the vertical line $\alpha = 1$, and that for α less than 1 the polarization reversal occurs in the L-X mode for $\omega^2 < \Omega_i^2$ and in the R-0 or R-X mode for $\Omega_i^2 (1 - 1/\mu + 1/\mu^2) < \omega^2 < \Omega_e^2$.

The mode in which the polarization reversal occurs are indicated in Figure 7, which summarizes the discussions given in this Section.

We conclude that for ULF and VLF waves in the magnetosphere the polarization reversal at θ satisfying (14) does not occur.

2.8. The lower hybrid resonance

We see from (6) that for propagation across the magnetic field, i.e., for $\theta = \frac{1}{2}\pi$, there is resonance at $S = 0$. As is indicated in Figures 1 and 4, there are two such resonances, and the one at lower frequency is called the lower hybrid resonance and the other at higher frequency the upper hybrid resonance.

Approximate expressions for the two hybrid resonance frequencies can be obtained by ignoring terms of order μ^{-1} compared with unity in the dispersion relation for $\theta = \frac{1}{2}\pi$. Stix (1962) gives for the lower hybrid resonance frequency ω_{LH}

$$1/\omega_{\text{LH}}^2 = 1/(\Omega_i^2 + \Pi_i^2) + 1/\Omega_i\Omega_e \quad (17)$$

and for the upper hybrid resonance frequency ω_{UH}

$$\omega_{\text{UH}}^2 = \Omega_e^2 + \Pi_e^2 \quad (18)$$

In the frequency range we are concerned here and for the plasma parameters appropriate to the magnetosphere the lower hybrid resonance frequency can be approximated to a good accuracy by the geometric mean of the ion and electron cyclotron frequencies:

$$\omega_{\text{LH}} = (\Omega_i\Omega_e)^{\frac{1}{2}} \quad (19)$$

A clear physical picture for this resonance was given by Auer, Hurwitz, Jr., and Miller (1958).

The lower hybrid resonance frequency in the magnetosphere at different distances from the earth's center is given in Table 1.

Table 1. The lower hybrid resonance frequency f_{LH} at various distances from the center of the earth.

r	f_{LH}
km	c/sec
10,000	5,260
15,000	1,560
20,000	657
25,000	337
30,000	195
35,000	123
40,000	82
45,000	58
50,000	42
55,000	32
60,000	24

2.9. The hydromagnetic approximation

When the wave frequency ω is well below the ion cyclotron frequency Ω_i , the quantities R and L in (10) and (11) are simplified and both R and L can be approximated by $1 + \gamma$, where $\gamma = 4 \pi \rho c^2 / B_0^2$; here $\rho = n_i m_i + n_e m_e$, i.e., the plasma density. With these approximations

for R and L the dielectric tensor defined in Section 2.1 becomes diagonal. The component K_{\perp} of the dielectric tensor perpendicular to the magnetic field then takes the well-known form (Spitzer, 1956)

$$K_{\perp} = 1 + \gamma$$

If α is large, as is the case with ULF waves in the magnetosphere, P in (12) can be approximated by $-\alpha$. With these approximations for R, L, and P the dispersion relation is simplified and readily factored, giving the following two modes. One of these modes gives

$$n^2 = 1 + \gamma \quad (20)$$

and the other

$$n^2 \cos^2 \theta = 1 + \gamma \quad (21)$$

In the first mode n^2 is independent of θ . For this reason Åström (1950) called this mode "ordinary" mode, and the second "extraordinary" mode. However, a closer examination shows that the first mode corresponds to the branch labeled R-X in Figure 4 and the second to that labeled L. Hence the exact expression for n^2 for the first mode depends on the magnetic field for $\theta = \frac{1}{2}\pi$. The problem of labeling the modes has already been discussed in Section 2.4.

By studying the ion velocity the mode corresponding to (20) can be shown to represent compressional wave, and the other mode (21) shear wave.

From a comparison of phase velocity for these two modes one finds that the compressional mode is the fast mode and that the shear mode is the slow mode.

From the continuity of the wave-normal surface we see that the Alfvén compressional mode (or the fast hydromagnetic mode) and the whistler mode belong to the same family. The Alfvén shear mode (or the slow hydromagnetic mode) disappears at the ion cyclotron frequency.

When $\gamma \gg 1$ the phase velocities for the compressional and shear modes recede to V_A and $V_A \cos \theta$, respectively, where $V_A = B_0 / \sqrt{4\pi\rho}$, which is usually called the Alfvén velocity. The condition that $\gamma \gg 1$ is equivalent to the condition that $V_A/c \ll 1$.

These approximations for the phase velocities can be readily obtained by a fluid-dynamical treatment of plasma with infinite conductivity and by neglecting displacement current.

3. Ray theory

3.1. Introduction

So far we have reviewed the wave modes in a cold plasma by studying the wave-normal surfaces. The basis for the study was the dispersion relation. We now investigate propagation of hydromagnetic waves from a somewhat different angle by constructing a ray theory. As the plane wave theory described in the preceding Sections has limitations in its application, the ray theory developed in the following Sections is valid only under certain conditions. However, just as the general discussions of wave modes are useful in understanding the propagation of waves, the theoretical study of the behavior of rays may be helpful in understanding some of the electromagnetic phenomena occurring in the magnetosphere.

Although the theoretical discussions in Sections 3.2 and 3.3 are of general nature, the theory is applied in Sections 3.4 to 3.8 to propagation of hydromagnetic waves in the magnetosphere.

3.2. The equations of motion of a ray

The basis of the theory is that the ray propagates with the group velocity. Hines (1951) and Auer, Hurwitz, Jr., and Miller (1958) have shown that the constructive interference maximum of a wave packet moves with the group velocity. We also assume that the mode in which the waves constituting the wave packet propagate is the same throughout its motion in the anisotropic medium. Coupling between different modes is assumed not to take place.

Denoting the position of a ray by \vec{r} and the group velocity by \vec{v}_g , we write the equation of motion for the ray as follows.

$$\dot{\vec{r}} = \vec{v}_g \quad (22)$$

where the dot signifies differentiation with time t . The group velocity \vec{v}_g is given by

$$\vec{v}_g = \partial \omega / \partial \vec{k} \quad (23)$$

The wave frequency ω and the wave vector \vec{k} are related by the dispersion relation which we write

$$D(\vec{k}, \omega, \vec{r}, t) = 0 \quad (24)$$

We introduce a parameter τ along the path of the ray. Then, using (23) and (24), the equation of motion (22) can be written in the following form.

$$\frac{d\vec{r}/d\tau}{dt/d\tau} = - \frac{\partial D / \partial \vec{k}}{\partial D / \partial \omega} \quad (25)$$

From our assumption D is constant along the trajectory, and hence we have

$$\delta D = \left(\frac{\partial D}{\partial \vec{k}} \cdot \frac{d\vec{k}}{d\tau} + \frac{\partial D}{\partial \omega} \frac{d\omega}{d\tau} + \frac{\partial D}{\partial \vec{r}} \cdot \frac{d\vec{r}}{d\tau} + \frac{\partial D}{\partial t} \frac{dt}{d\tau} \right) = 0 \quad (26)$$

For (26) to hold for any τ the content in the parentheses must be zero. We group the four terms in the parentheses in (26) as follows:

$$\left(\frac{\partial D}{\partial \vec{k}} \cdot \frac{d\vec{k}}{d\tau} + \frac{\partial D}{\partial \vec{r}} \cdot \frac{d\vec{r}}{d\tau} \right) + \left(\frac{\partial D}{\partial \omega} \frac{d\omega}{d\tau} + \frac{\partial D}{\partial t} \frac{dt}{d\tau} \right) = 0 \quad (27)$$

If each of the two factors in (27) is zero, the required condition (26) is satisfied. Equations (25) and (27) are satisfied by the following set of equations:

$$d\vec{r}/d\tau = \partial D / \partial \vec{k} \quad (28)$$

$$d\vec{k}/d\tau = - \partial D / \partial \vec{r} \quad (29)$$

$$dt/d\tau = - \partial D / \partial \omega \quad (30)$$

$$d\omega/d\tau = \partial D / \partial t \quad (31)$$

If D is independent of time, the last equation (31) states that ω is conserved along the ray trajectory. The third equation (30) gives the relation between time t and parameter τ .

The above set of equations clearly indicates an analogy between the ray theory and classical mechanics. The wave vector \vec{k} and the frequency ω of a ray play the roles of the momentum and the energy of a particle, respectively. However, this analogy does not enable us to formulate the ray theory in Hamiltonian form. This is because the motion of a ray corresponds to that of a particle of zero mass, and hence it is expected that the Lagrangian for the ray is identically zero. In the end of the following Section we will show that the Lagrangian indeed vanishes.

However, when Fermat's principle is valid the problem can be formulated in Hamiltonian form. Hence we now examine under what conditions Fermat's principle is consistent with our formulation.

3.3. Fermat's principle

Weinberg (1962) showed that when the eikonal is stationary, the principle of least time, i.e., Fermat's principle, holds if the dispersion relation is homogeneous in \vec{k} and ω . In this Section we derive the same condition by pursuing the formulation in the preceding Section.

In classical mechanics the principle of least action holds when the Hamiltonian is conserved. We limit ourselves to the case when the frequency ω is conserved along the path, that is, D is conserved along the path.

We first define the action A for the ray by the integral

$$A = \int_{t_1}^{t_2} \vec{k} \cdot \dot{\vec{r}} dt \quad (32)$$

where the dot means, as before, differentiation with t .

Next, we calculate the variation ΔA , where the Δ -variation differs from the δ -variation appearing in virtual displacement; in the latter, time is kept unchanged, whereas in the former the process involves a change dt (see, e.g., Goldstein, 1951). For any function f of \vec{r} and t , the Δ -variation of f is

$$\begin{aligned} \Delta f &= d\tau \left(\frac{\partial f}{\partial \tau} + \dot{\vec{r}} \cdot \frac{d\vec{r}}{d\tau} \right) \\ &= \delta f + \dot{\vec{r}} \Delta t \end{aligned} \quad (33)$$

In particular,

$$\Delta \vec{r} = \delta \vec{r} + \dot{\vec{r}} \Delta t \quad (34)$$

Applying the Δ -variation to (32) we have

$$\Delta A = \int_{t_1}^{t_2} \delta (\vec{k} \cdot \dot{\vec{r}}) dt + \left. \vec{k} \cdot \dot{\vec{r}} \Delta t \right|_{t_1}^{t_2} \quad (35)$$

The first integral can be calculated in the following way:

$$\begin{aligned}
 \int_{t_1}^{t_2} \delta (\vec{k} \cdot \dot{\vec{r}}) dt &= \int_{t_1}^{t_2} \delta \vec{k} \cdot \dot{\vec{r}} dt + \int_{t_1}^{t_2} \vec{k} \cdot \delta \dot{\vec{r}} dt \\
 &= \int_{t_1}^{t_2} \delta \vec{k} \cdot \dot{\vec{r}} dt - \int_{t_1}^{t_2} \dot{\vec{k}} \cdot \delta \vec{r} dt + \vec{k} \cdot \delta \vec{r} \Big|_{t_1}^{t_2} \\
 &= \int_{t_1}^{t_2} (\delta \vec{k} \cdot \dot{\vec{r}} - \dot{\vec{k}} \cdot \delta \vec{r}) dt - \vec{k} \cdot \dot{\vec{r}} \Delta t \Big|_{t_1}^{t_2}
 \end{aligned}$$

Here we used the fact that the order of the δ - and dot-operation can be interchanged, and partial integration was performed on the second integral on the right-hand side of the first line. To obtain the last result we used (34) and the condition that $\Delta \vec{r} = 0$ at the end points.

Thus (35) reduces to

$$\Delta A = \int_{t_1}^{t_2} (\delta \vec{k} \cdot \dot{\vec{r}} - \dot{\vec{k}} \cdot \delta \vec{r}) dt$$

Using (22), (23), (28), (29), and (30), the integrand can be transformed as follows:

$$\begin{aligned}
 \delta \vec{k} \cdot \dot{\vec{r}} - \dot{\vec{k}} \cdot \delta \vec{r} &= - (\partial D / \partial \omega)^{-1} \left(\delta \vec{k} \cdot \frac{\partial D}{\partial \vec{R}} + \delta \dot{\vec{r}} \cdot \frac{\partial D}{\partial \dot{\vec{r}}} \right) \\
 &= - (\partial D / \partial \omega)^{-1} \delta D \\
 &= 0
 \end{aligned}$$

Thus we have proved that

$$\Delta A = 0$$

Namely, in our system the principle of least action holds if the action is defined by (32). Having proved this principle we go back to the expression for ΔA given in (35). If

$$\vec{k} \cdot \vec{r} = \text{constant} \neq 0 \quad (36)$$

then (35) reduces to

$$\Delta(t_2 - t_1) = 0$$

which implies the principle of least time, or Fermat's principle. The condition (36) can be rewritten as follows:

$$-(\vec{k} \cdot \partial D / \partial \vec{k}) / (\partial D / \partial \omega) = \text{constant} \quad (37)$$

A sufficient condition for (37) to hold is that D is homogeneous in \vec{k} and ω , because if D is homogeneous in \vec{k} and ω , i.e., if

$$D(\alpha \vec{k}, \alpha \omega) = \alpha^n D(\vec{k}, \omega)$$

Euler's homogeneity equation becomes

$$\vec{k} \cdot \frac{\partial D}{\partial \vec{k}} + \omega \frac{\partial D}{\partial \omega} = nD = 0 \quad (38)$$

Thus the constant in (37) takes the value of ω .

The homogeneity equation (38) can be transformed into the form

$$\vec{v}_g \cdot \frac{\vec{k}}{\omega} = 1$$

which implies the equality of the group and phase velocities.

It is pointed out here that the action (32) is the same as the eikonal S in Weinberg's formulation, and that the principle of least action derived here is equivalent to the principle of stationary S in Weinberg's eikonal theory.

For the Alfvén compressional mode the dispersion relation is homogeneous in \vec{k} and ω , and hence Fermat's principle holds. As a matter of fact, for this mode the group velocity is equal to the phase velocity. However, for the shear mode the dispersion relation is not homogeneous in the components of \vec{k} , and thus Fermat's principle does not hold. As has been noted by Weinberg (1962), the application of Fermat's principle by Francis, Green and Dessler (1959) is justified.

In concluding this Section a remark is made on the Lagrangian. In classical mechanics the Lagrangian L is related to the Hamiltonian by

$$L = \vec{p} \cdot \dot{\vec{r}} - H$$

where \vec{p} is the momentum.

If we define the Lagrangian for the ray by

$$L = \vec{k} \cdot \dot{\vec{r}} - \omega$$

then from (36) our Lagrangian is identically zero, confirming our expectation expressed in Section 3.2. Thus the ray theory cannot be constructed in Hamiltonian form using the Lagrangian defined above.

3.4. A ray theory for modes with isotropic phase velocity

In this and the following Sections we discuss the case in which the phase velocity is isotropic. We specifically study propagation of a hydro-magnetic ray. For the Alfvén compressional mode the group velocity is the same as the phase velocity. Hence we simply refer to these velocities by the single term the Alfvén velocity.

Fermat's principle states that the motion of a ray from a point P_1 to another point P_2 is such that the variation of the line integral $\int_{P_1}^{P_2} ds/V$ for fixed P_1 and P_2 is zero, i.e.,

$$\delta \int_{P_1}^{P_2} ds/V(r, \theta, \phi) = 0 \quad (39)$$

where $V(r, \theta, \phi)$ is the Alfvén velocity. We use a spherical coordinate system (r, θ, ϕ) in this and following Sections; when we refer to the magnetosphere the origin of the spherical coordinate system is taken to coincide with the earth's center. In the preceding Sections θ was the angle which \vec{k} makes with the magnetic field, but in the rest of the paper θ is the polar angle.

We write (39) in the form:

$$\delta \int_{t_1}^{t_2} \frac{(\dot{r}^2 + r^2 \dot{\theta}^2 + r^2 \dot{\phi}^2 \sin^2 \theta)^{1/2}}{V(r, \theta, \phi)} dt = 0 \quad (40)$$

where t_1 and t_2 are the times when the ray is at P_1 and P_2 , and where the dot means differentiation with respect to time t .

Equation (40) is formally the same as the variation equation expressing

Hamilton's principle for a system whose Lagrangian is equal to the integrand in (40). Thus we take the integrand of (40) as the Lagrangian of our system, and define the generalized momenta conjugate to r , θ , ϕ by

$$p_k = \partial L / \partial \dot{q}_k \quad (k = 1, 2, 3)$$

where it is understood that the subscript k refers to r , θ , ϕ components and that q_k ($k = 1, 2, 3$) represents r , θ , ϕ , respectively.

The Hamiltonian H of the system is

$$\begin{aligned} H &= \sum_k p_k \dot{q}_k - L \\ &= V(r, \theta, \phi)^2 \left[p_r^2 + p_\theta^2 / r^2 + p_\phi^2 / (r^2 \sin^2 \theta) \right] - 1 \end{aligned}$$

Then the canonical equations can readily be formed. Stegelmann and von Kenschitzki (1964) proceeded to integrate the canonical equations numerically.

3.5. Axially symmetric case: allowed and forbidden regions for a ray

It is obvious that if the Alfvén velocity is independent of ϕ , the Hamiltonian does not contain ϕ explicitly; thus, ϕ is a cyclic coordinate. It follows that the conjugate momentum p_ϕ is a constant of motion. From the definition of p_ϕ we immediately obtain the equation

$$(r^2 \dot{\phi} \sin^2 \theta) / V(r, \theta)^2 = \text{constant} \quad (41)$$

This equation, of course, is the canonical equation for ϕ with p_ϕ constant.

Since $\dot{\phi} = V d\phi/ds$, where s is path length along the trajectory, (41) can be written as follows:

$$(R^2/V) d\phi/ds = \alpha \quad (42)$$

where

$$R = r \sin \theta \quad (43)$$

and where α is a constant.

We define an angle χ by the equation

$$R d\phi/ds = \sin \chi \quad (44)$$

so that χ is the angle between the tangent to the ray in the direction of its motion and the meridian plane. As can be seen in (44) the sign of χ is taken such that χ is positive when ϕ increases as the ray advances. Figure 8 illustrates the angle χ .

Using χ , (42) reduces to

$$(R/V) \sin \chi = \alpha \quad (45)$$

For rays belonging to α , (45) gives the angle χ as a function of r and θ .

Since $-1 \leq \sin \chi \leq 1$, we have the relation

$$-1 \leq \alpha V/R \leq 1 \quad (46)$$

Thus, given the value of α , (46) defines the "allowed" region for the rays belonging to α . Areas outside the allowed region are forbidden to these rays.

The constant α can be taken as the initial condition specified by r_0 , θ_0 , and χ_0 :

$$\alpha = (R_0/V_0) \sin \chi_0 \quad (47)$$

where R_0 and V_0 are the values of R and V at r_0, θ_0 .

It should be noted that the angle χ_0 does not specify the initial direction of a ray completely, except in the equatorial plane. To specify the initial direction of a ray completely one more angle is needed (Section 3.8); however, we only need χ_0 for the time being.

When the initial conditions r_0, θ_0 , and χ_0 are given, the allowed and forbidden regions can be mapped out using (46) without integrating the equations of motion.

The problem is formally identical with that in Störmer's work on the motion of a charged particle in a dipole magnetic field (Störmer, 1955). In Störmer's problem also the Hamiltonian does not contain ϕ explicitly.

The meaning of (44) becomes more explicit if we limit ourselves to rays confined in the equatorial plane. The Alfvén velocity V is now a function of r alone, and χ is the angle which the tangent to the ray trajectory makes with the radial direction. Let χ be measured positively from the inward radial direction toward the direction of increasing ϕ (which is taken to be eastward) and let χ vary from $-\pi$ to π ; thus rays with $-\frac{1}{2}\pi < \chi < \frac{1}{2}\pi$ are inbound and those with $|\chi| > \frac{1}{2}\pi$ are outbound, and when $\chi = \pm\frac{1}{2}\pi$, a ray is tangent to the circle of radius r .

The angle χ at r is related to its initial value χ_0 at the point source at r_0 by

$$\sin \chi = (r_0/r) (V/V_0) \sin \chi_0$$

If $V(r)$ is a maximum at $r = r_m$ and is a monotonically decreasing function of r with increasing r , then for $r_0 > r > r_m$, the inequality $|\chi| > |\chi_0|$ always

holds. This simply implies the obvious result that the ray is bent away from the region of high Alfvén velocity.

The Alfvén velocity is a maximum at several thousand kilometers altitude and decreases both above and below this level (Dessler, 1958). The Alfvén velocity increases again near the F₂ peak, but we are not concerned here with the propagation of hydromagnetic waves in the ionosphere. We only consider the ray trajectories above 600 km altitude.

It is of interest to find the critical initial angle $\chi_{o,c}$ at which an inbound ray from a point source at a great distance is reflected away from the earth at the region ($r = r_m$) of the Alfvén velocity maximum. This critical initial angle can be determined by

$$|\sin \chi_{o,c}| = (r_m/r_o) (V_o/V_m)$$

where V_m is the value of V at r_m .

For a rough estimate, taking $r_o = 60,000$ km, $r_m = 10,000$ km, and $V_o = 400$ km/sec, $V_m = 2,000$ km/sec, we obtain $|\sin \chi_{o,c}| = 1/30$, and hence $|\chi_{o,c}|$ is about 1.9° . There are uncertainties in the distribution of Alfvén velocity in the magnetosphere, but $\chi_{o,c}$ is not likely to be changed greatly as more accurate information on the Alfvén velocity distribution becomes available.

3.6. A further remark on ray tracing in the equatorial plane

In Section 3.5, time t was used for the variable in the variation equation. However, any one of the three coordinates can be used as the variable in place of t .

If we choose ϕ as the variable, and if we confine ourselves to the equatorial plane, the integrand L in the variation equation reduces to

$$L(r, r') = (r'^2 + r^2)^{\frac{1}{2}} / V(r)$$

where the prime represents differentiation with respect to ϕ .

Considering this function as the Lagrangian, Lagrange's equation of motion is

$$\frac{d}{d\phi} \left(\frac{\partial L}{\partial r'} \right) - \frac{\partial L}{\partial r} = 0$$

This is the equation used by Francis, Green and Dessler (1959).

Denoting the momentum conjugate to r by p , the Hamiltonian for the system is given by

$$H = p r' - L$$

where

$$p = \partial L / \partial r'$$

It is understood that H is expressed as a function of r and p . Then the Hamiltonian does not contain ϕ explicitly. Thus the Hamiltonian is a constant of motion. We immediately arrive at the equation:

$$r' \frac{\partial L}{\partial r'} - L = \text{constant}$$

This is the equation which Francis, Green and Dessler (1959) derived mathematically and used for their calculation of the transit time for the ray, and which Dessler, Francis, and Parker (1960) used for their two dimensional ray tracing.

3.7. Hydromagnetic rays in the magnetosphere: axially symmetric case

Using the method described in Section 3.5, we will now investigate the accessibility of hydromagnetic rays originating from the magnetospheric boundary to the vicinity of the earth. We use the same model magnetosphere as the one presented in Section 2.5; for the magnetic field we approximate the geomagnetic field by a centered dipole.

As was shown in Section 3.5, when the position (r_0, θ_0) of the point source and the initial value of χ of the ray are specified, we can determine the allowed and forbidden regions by (46) and (47).

We place the point source at the distance of 10 earth-radii from the earth's center, i.e., $r_0 = 10a$, where a is the earth's radius, and we determine allowed and forbidden regions for $\theta_0 = 30^\circ$, 60° , and 90° ; the last value of θ_0 places the source on the equatorial plane.

Typical diagrams showing the allowed and forbidden regions are presented in Figure 9. In the Figure, forbidden regions are indicated by patches and the open areas represent allowed regions. The patched circle in the center represents the earth and the position of the point source can be at any of the four arrows on the great circle whose radius is ten times that of the earth. All the diagrams are symmetric with respect to the equator, and the three dimensional allowed (or forbidden) region can be obtained by rotating each diagram about the vertical axis through the center, namely, the dipole axis.

For very small values of χ_0 (well below 1° , say), that is, when the initial direction of the ray deviates from the meridian plane only by a small angle, the ray can reach the earth's vicinity except directly above the poles.

As χ_0 increases the two forbidden regions around the axis, one in each hemisphere, become larger and extend to lower latitudes near the altitude of the Alfvén velocity maximum. When χ_0 reaches some critical value, the tips of the northern and southern forbidden regions touch each other on the equatorial plane. There is an allowed region between the ionosphere and the altitude at which the joining of the two forbidden regions takes place on the equatorial plane, but this inner allowed region is not accessible to the ray coming from outside.

When χ_0 exceeds the critical value, the earth is completely immersed in a forbidden region and the outer allowed region is more and more pushed outward, and finally, as χ_0 tends to 90° its inner surface approaches some limiting surface which intersects the large sphere (of radius r_0) at $\theta = \theta_0$ and $\theta = \pi - \theta_0$. When θ_0 is 90° , the allowed region for $\chi_0 = 90^\circ$ degenerates to a circle of radius r_0 on the equatorial plane.

The critical value of χ_0 becomes smaller as θ_0 increases; for $\theta_0 = 30^\circ$, 60° , and 90° , the critical χ_0 is 3.3° , 1.4° , and 0.9° , respectively. In Figure 9 the diagrams for these critical circumstances are included.

For $\chi_0 = 10^\circ$, 30° , 60° , and 90° the forbidden regions are indicated in one diagram for each θ_0 .

We conclude that the earth and its immediate vicinity are remarkably well protected from the hydromagnetic rays generated in the outer regions of the magnetosphere. This feature has been shown by Stegelmann and von Kenschitzki (1964) with their results from numerical ray tracing.

3.8. Hydromagnetic rays in the distorted magnetosphere: axially asymmetric case

The magnetosphere is contained in a cavity in the streaming solar plasma (Cahill and Amazeen, 1963; Ness et al., 1964). A number of workers have attempted to theoretically determine the shape of the boundary of the magnetosphere (for reference, see a review paper by Beard, 1964).

In this Section we only briefly discuss the effect of the distortion of the magnetosphere on the propagation of hydromagnetic waves.

In the absence of symmetry we have to write down the equations of motion and solve them by some numerical method.

For the sake of convenience we multiply the Hamiltonian given in Section 3.4 by the factor $\frac{1}{2}$. With this Hamiltonian the canonical equations are

$$\begin{aligned}\dot{r} &= V^2 p_r \\ \dot{\theta} &= V^2 p_\theta / r^2 \\ \dot{\phi} &= V^2 p_\phi / (r^2 \sin^2 \theta) \\ \dot{p}_r &= -(1/V) \partial V / \partial r + (V^2 / r^3) (p_\theta^2 + p_\phi^2 / \sin^2 \theta) \\ \dot{p}_\theta &= -(1/V) \partial V / \partial \theta + (V^2 / r^2) p_\phi^2 \cos \theta / \sin^3 \theta \\ \dot{p}_\phi &= -(1/V) \partial V / \partial \phi\end{aligned}\tag{48}$$

These equations are not completely independent. The Hamiltonian of the system is identically zero, and we have

$$p_r^2 + p_\theta^2 / r^2 + p_\phi^2 / (r^2 \sin^2 \theta) = 1/V^2\tag{49}$$

Using (49) one of the variables can be eliminated from the set of equations (48). But it is found convenient to use (49) as a check in the numerical ray tracing calculation.

We define the direction of the tangent to the ray trajectory at a point P by two angles χ and η . The angle χ is the same as that defined in the preceding Section, and η is the angle which the tangent to the projection of the trajectory onto the meridian plane makes with the radial direction, namely,

$$\sin \chi = (d\phi/ds) r \sin \theta$$

$$\cos \eta = -(dr/ds) \sec \chi$$

We denote the initial values of χ and η at (r_0, θ_0, ϕ_0) by χ_0 and η_0 , respectively.

The initial values of the momenta can be written in terms of $r_0, \theta_0, \phi_0, \chi_0, \eta_0$, and $V(r_0, \theta_0, \phi_0)$.

For the deformed geomagnetic field we take the model proposed by Mead (1964). For the dipole field we take $g_1^0 = -0.31$ gauss, and for the additional field due to the deformation we take

$$\bar{g}_1^0 = -0.2515 / r_b^3 \text{ gauss}$$

$$\bar{g}_2^1 = 0.1215 / r_b^4 \text{ gauss}$$

where g 's are well-known Gauss coefficients in the spherical harmonic expansion of the magnetic field, and where r_b is the distance, measured in earth-radii, from the earth's center to the boundary of the magnetosphere at the subsolar point. Here r_b is taken to be 10 earth-radii.

A computer program has been developed to integrate the equations of motion (48) with $r_0, \theta_0, \phi_0, \chi_0$, and η_0 as the initial conditions. For integration the Runge-Kutta method was used.

In this paper, trajectories on the equatorial plane alone are discussed.

Figure 10 shows typical examples of the trajectories in the equatorial plane. The position of the point source is placed at 10 earth-radii regardless of the longitude. This assumption is made because the location of the magnetospheric boundary is not well known on the dark side of the magnetosphere, and because with a fixed r_0 we can compare trajectories starting from sources at different longitudes more directly. Here longitude, ϕ , is measured eastward from the midnight meridian; in Figure 10 the midnight meridian is towards the left and the longitude increases counterclockwise.

In the lower half of Figure 10, trajectories starting at $\phi_0 = 0^\circ, 45^\circ, 135^\circ, \text{ and } 180^\circ$, all with $\chi_0 = 0$ (i.e., rays directed initially towards the origin) are shown. In the upper half, trajectories with their initial position at $\phi_0 = 90^\circ$ with $\chi_0 = 0, 1^\circ, 3^\circ, 4^\circ, 5^\circ, 6^\circ, \text{ and } 7^\circ$ are drawn.

The effect of the distortion of the magnetosphere on the ray trajectories can be described by saying that hydromagnetic rays tend to be 'blown' towards the direction away from the sun. This is because the magnetic field is more compressed on the sunlit side of the magnetosphere than on its dark side, thus increasing the Alfvén velocity in the region facing the sun.

However, the results presented in this Section should be interpreted with caution. Although the distortion of the geomagnetic field is taken into account, possible changes in the plasma density distribution associated with the distortion are not considered here. Appreciable asymmetry may be introduced in the plasma density, but no observational data are available as yet that indicate such an effect.

The magnetic field configuration on the dark side of the magnetosphere has also not as yet been established. Since the trajectories are sensitive to large scale magnetic field patterns, the actual trajectories in the magnetosphere may be different from those shown in this paper. Our purpose is to demonstrate qualitative characteristics of ray trajectories in the magnetosphere. However, for the model used in this Section the calculations are made as accurately as possible within the practical limitations.

It is observed in Figure 10 that if the point source is not in the meridian containing the sun (i.e., $\phi_0 = 0^\circ$ or 180°), the ray directed initially towards the origin does not reach the earth. For the ray to reach the earth it must start with χ_0 slightly greater than 0. If χ_0 becomes too large, the ray is bent back at the region of Alfvén velocity maximum. This circumstance is shown for $\phi_0 = 90^\circ$ in the upper half of Figure 10. At this ϕ_0 , rays with $\chi_0 = 3.0^\circ$ and less are 'blown' towards the back of the magnetosphere. At χ_0 between 3.0° and 3.2° the ray begins to penetrate into the immediate vicinity of the earth, and this condition prevails till χ_0 reaches a value a little less than 6.5° . Beyond this latter angle the ray is again reflected away from the earth at the region of Alfvén velocity maximum.

In Figure 10 the time in seconds is indicated along the trajectories. It is of interest to compare the transit time from r_0 to some altitude near the earth for the trajectory in the midnight meridian with the corresponding transit time for the trajectory in the noon meridian. In Figure 10 the altitude of the point marked 95 seconds in the noon meridian and that of

the point marked 129 seconds in the midnight meridian are within 45 km from each other. The mean of the two altitudes is 1,363 km above the earth's surface. Thus the difference in the transit time from 10 earth-radii to this altitude is about 34 seconds.

However, as has already been mentioned, caution should be exercised in applying this result to any actual events that occur in the magnetosphere.

In concluding the discussions of the ray theory the following remarks are made. The hydromagnetic approximation is based on the condition that $\omega \ll \Omega_i$. Thus for the most part of the magnetosphere this approximation is good below 10 c/sec (Figure 4). There is another limitation to the ray theory, namely, that the wavelength be short compared with the dimension under consideration. We put this condition in the form $\omega \gg V/L$, where L is the typical scale length. If we take L to be the smallest value of the radius of curvature for the ray trajectories, then the minimum frequency may be set at about 1 c/sec. Thus, roughly speaking, the ray theory is applicable to propagation of hydromagnetic waves of frequencies about 1 to 10 c/sec.

A more extensive study of the ray trajectories in the magnetosphere and their physical implications will be reported later. For instance, the efficiency of energy transfer from solar winds to the ionosphere via hydromagnetic waves is considerably reduced by the limited accessibility of the hydromagnetic waves to the immediate vicinity of the earth.

A theoretical study of geometrical hydromagnetics based on a classical hydromagnetic fluid has been made by Bazer and Hurley (1963); their paper includes comprehensive reference to the literature on the subject.

4. Conclusions

We reviewed the possible modes of waves in a two-component cold plasma using the Clemmow-Mullaly-Allis diagram. A systematic method of labeling the modes was explained.

The modes relevant to propagation of ULF and VLF waves in the regions of plasma parameter space representing the conditions in the magnetosphere were reviewed. For frequencies below the ion cyclotron frequency there are two modes: the fast mode with right-handed circular polarization for propagation along the magnetic field and with phase velocity dependent on the magnetic field for propagation across it, and the slow mode with left-handed circular polarization for propagation along the magnetic field. Waves in the latter mode do not propagate across the magnetic field. Above the ion cyclotron frequency, only the fast mode represents propagating wave, and above the lower hybrid resonance frequency this mode becomes the whistler mode.

Reversal of polarization (in the electric field) depending upon the direction of phase propagation with reference to the direction of the magnetic field was discussed. We concluded that there is no such reversal in polarization in ULF and VLF waves in the magnetosphere.

The hydromagnetic approximation was examined and its relation to the more exact treatment was indicated.

In this paper we only discussed propagation of waves in a collisionless plasma. When the thermal motions of electrons and ions are included, the waves found in a cold plasma are modified. The modifications are often only slight, but in a hot plasma new modes are introduced which have no

counterpart in a cold plasma. There are two such modes in a relatively low frequency range. They are ion acoustic waves and electrostatic ion cyclotron waves. These waves were not discussed in this paper; the reader is referred to discussions on these waves made, for instance, by Spitzer (1956), Bernstein (1958) and Stix (1962).

In the latter half of this paper, we changed the line of approach, and formulated a ray theory. The equations of motion of a ray were derived from a simple postulate that a ray moves with the group velocity. The action of the ray was defined in analogy with classical mechanics, and the principle of least action was proved. It was shown that the principle of least action takes the form of the principle of least time when the dispersion relation is homogeneous in the wave vector \vec{k} and the frequency ω .

For the case in which the wave-normal surface is spherical, a ray theory was formulated in Hamiltonian form. In the axially symmetric case the generalized momentum conjugate to the azimuthal coordinate becomes a constant of motion. Using this relation, allowed and forbidden regions were defined for a hydromagnetic ray in the magnetosphere with the magnetic field approximated by that of a dipole. It was shown that a ray originating from the magnetospheric boundary can reach the ionosphere only if the deviation of the initial direction of the ray from the meridian plane is small.

When the distortion of the geomagnetic field due to solar wind is taken into account, the ray trajectories in the magnetosphere are appreciably altered from those in a dipole field.

In spite of the limitations in its application the hydromagnetic ray

theory for the magnetosphere should provide a guide towards a more complete understanding of propagation of hydromagnetic waves in the magnetosphere.

Acknowledgements

I wish to thank Mr. W. F. Cahill for his valuable suggestions on the numerical calculations in this paper. I am indebted to Mr. W. H. Mish, Mrs. S. J. Hendricks, and Mrs. P. J. Connor for their helpful assistance in preparing the computer programs and performing the calculation.

References

- Alfvén, H. (1942), On the existence of electromagnetic-hydromagnetic waves, *Arkiv f. Mat.*, 29 B, No. 2; Existence of electromagnetic-hydromagnetic waves, *Nature*, 150, 405-406.
- Allis, W. P. (1959), Waves in a plasma, *Sherwood Conf. Contr. Fusion, Gatlinburg*, Apr. 27-28, p.32, TID-7582.
- Allis, W. P., S. J. Buchsbaum, and A. Bers (1963), *Waves in anisotropic plasmas* (MIT Press, Cambridge, Mass.)
- Åström, E. O. (1950), On waves in an ionized gas, *Arkiv f. Fysik*, 2, No. 42, 443-457.
- Auer, P. L., H. Hurwitz, Jr., and R. D. Miller (1958), Collective oscillations in a cold plasma, *Phys. Fluids*, 1, No. 6, 501-514.
- Bazer, J., and Hurley, J. (1963), Geometrical hydromagnetics, *J. Geophys. Res.*, 68, No. 1, 147-174.
- Beard, D. B. (1964), The solar wind geomagnetic field boundary, *Rev. Geophys.*, 2, No. 2, 335-365.
- Bernstein, I. B. (1958), Waves in a plasma in a magnetic field, *Phys. Rev.*, 109, No. 1, 10-21.
- Cahill, L. J., and P. G. Amazeen (1963), The boundary of the geomagnetic field, *J. Geophys. Res.*, 68, No. 7, 1835-1843.
- Clemmow, P. C., and R. F. Mullaly (1955), Dependence of the refractive index in magneto-ionic theory on the direction of the wave normal, "Physics of the Ionosphere: Report of Phys. Soc. Conf., Cambridge, Sept. 1954", 340-350, *Phys. Soc.*, London.

- Dessler, A. J. (1958), The propagation velocity of world-wide sudden commencements of magnetic storms., J. Geophys. Res., 63, No. 2. 405-408.
- Dessler, A. J., W. E. Francis, and E. N. Parker (1960), Geomagnetic Storm sudden commencement rise times, J. Geophys. Res., 65, No. 9, 2715-2719.
- Francis, W. E., M. I. Green, and A. J. Dessler (1959), Hydromagnetic propagation of sudden commencements of magnetic storms, J. Geophys. Res., 64, No. 10, 1643-1645.
- Goldstein, H. (1951), Classical mechanics (Addison-Wesley Press, Inc., Cambridge, Mass.)
- Hines, C. O. (1951), Wave packets, the Poynting vector, and energy flow: Part II-group propagation through dissipative isotropic media, J. Geophys. Res., 56, No. 2, 197-206.
- Liemohn, H. B., and F. L. Scarf (1964), Whistler determination of electron energy and density distributions in the magnetosphere, J. Geophys. Res., 69, No. 5, 883-904.
- Mead, G. D. (1964), Deformation of the geomagnetic field by the solar wind, J. Geophys. Res. 69, No. 7, 1181-1195.
- Ness, N. F., C. S. Scarce, and J. B. Seek (1964), Initial results of the IMF-I magnetic field experiment, NASA-Goddard Space Flight Center, X-612-64-95, Apr. 1964.
- Sitenko, A. G., and K. N. Stepanov (1957), On the oscillations of an electron plasma in a magnetic field, Soviet Phys. JETP, 4, No. 4, 512-520.

- Spitzer, L., Jr., (1956), Physics of fully ionized gases (Interscience Publishers, Inc., New York, N. Y.)
- Stegelmann, E. J., and C. H. von Kenschitzki (1964), On the interpretation of the sudden commencement of geomagnetic storms, J. Geophys. Res., 69, No. 1, 139-155.
- Stix, T. H. (1962), The theory of plasma waves (McGraw-Hill Book Co., Inc., New York, N. Y.).
- Störmer, C. (1955), The polar aurora, Part II, Chs. I and II (Oxford Univ. Press, Oxford).
- Weinberg, S. (1962), Eikonal method in magnetohydrodynamics, Phys. Rev., 126, No. 6, 1899-1909.

Figures

- Figure 1. The CMA diagram for a two-component cold plasma, showing the topological characteristics of the wave-normal surfaces.
- Figure 2. The electron density distribution in the model magnetosphere used in this paper.
- Figure 3. The electron cyclotron frequency and the electron plasma frequency as functions of distance from the earth's center.
- Figure 4. The CMA diagram for ULF and VLF waves in the model magnetosphere.
- Figure 5. Areas in the plasma parameter plane in which the polarization reversal can occur at θ satisfying (14).
- Figure 6. Illustrating the solutions to $RL + PS - 2S^2 = 0$.
- Figure 7. The modes in which polarization reversal occurs at θ satisfying (14).
- Figure 8. Illustrating the angle χ .
- Figure 9. Allowed and forbidden regions for a hydromagnetic ray in the magnetosphere with a dipole field.
- Figure 10. Illustrating ray trajectories in the equatorial plane in the distorted magnetosphere.

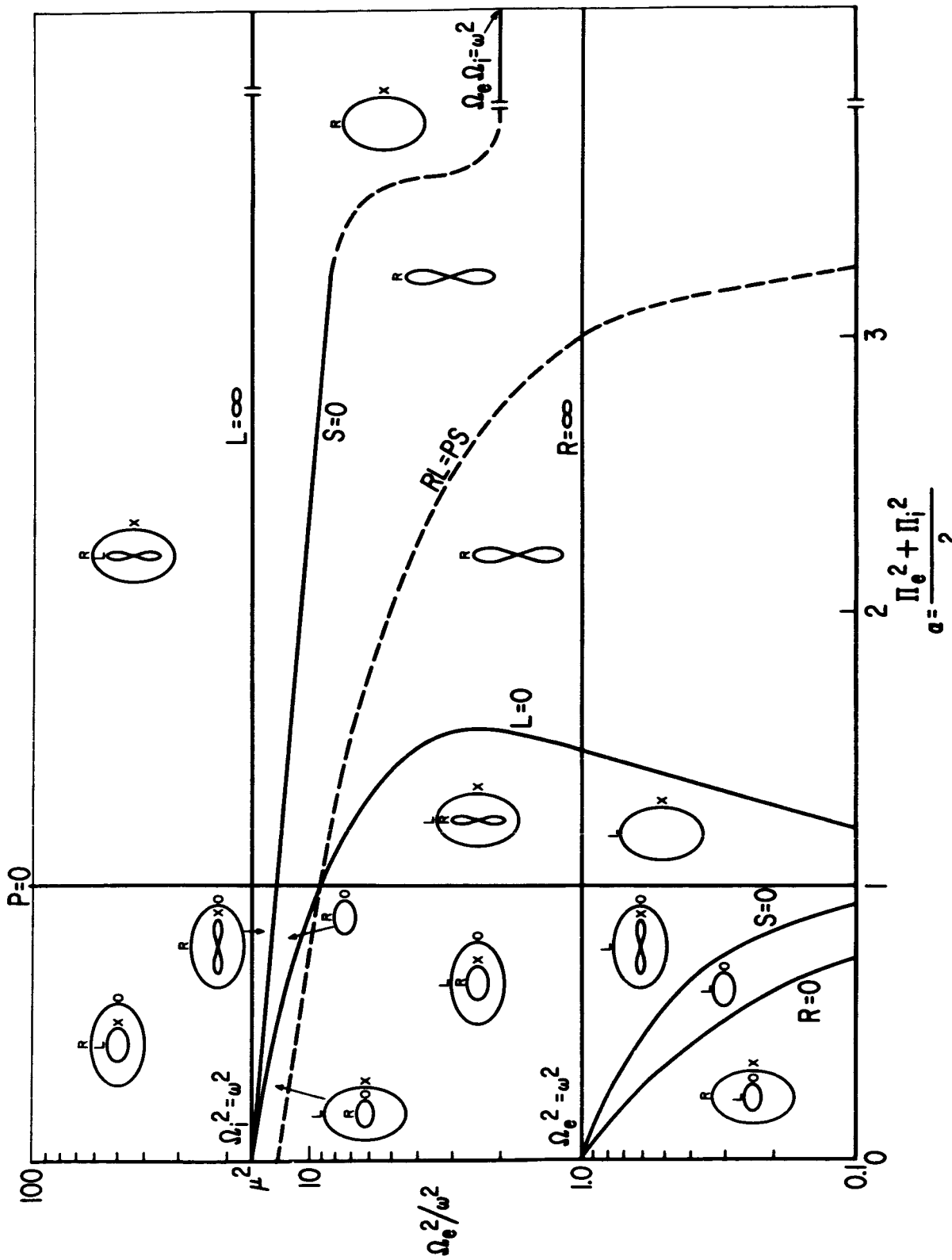


Figure 1.

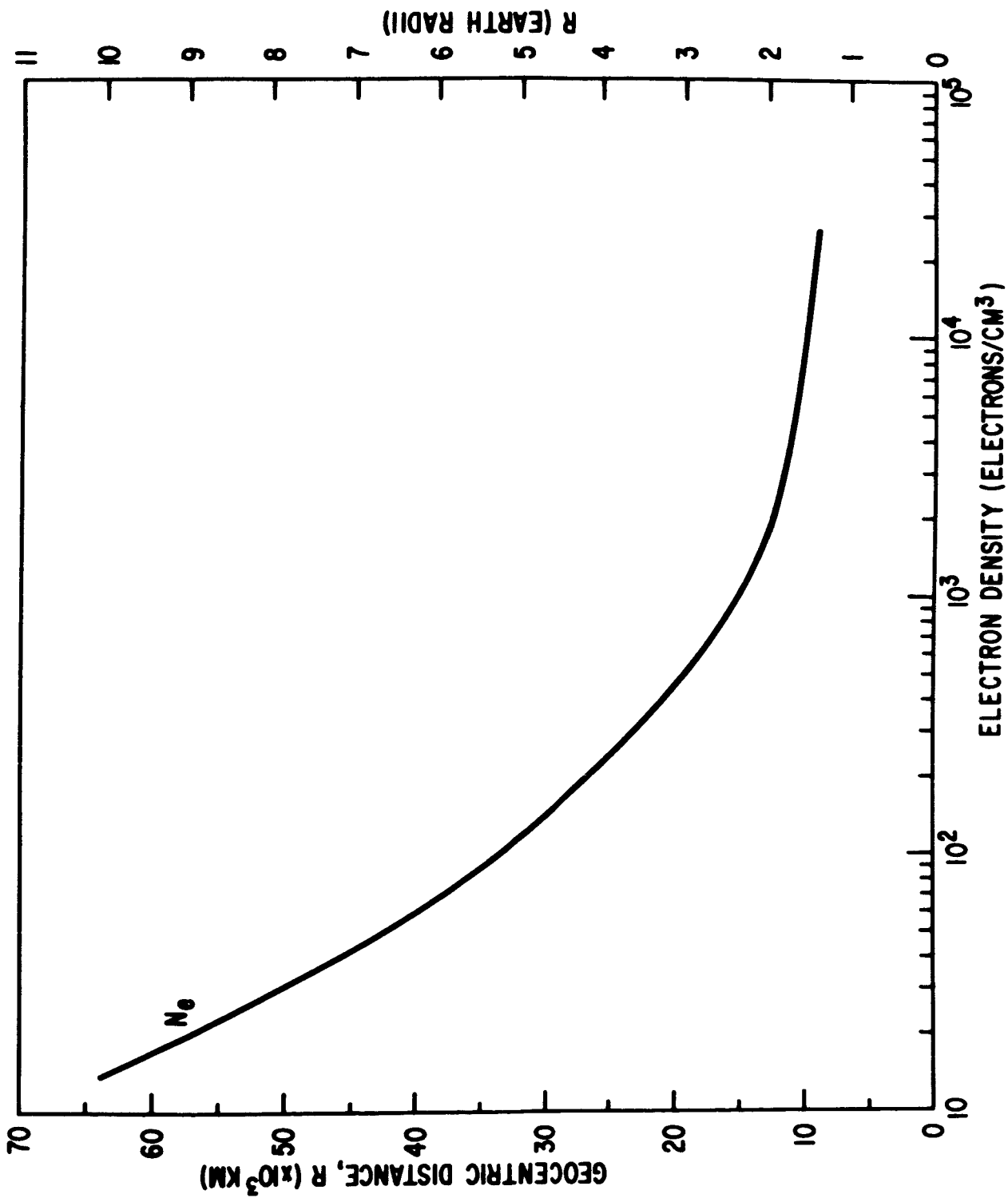


Figure 2.

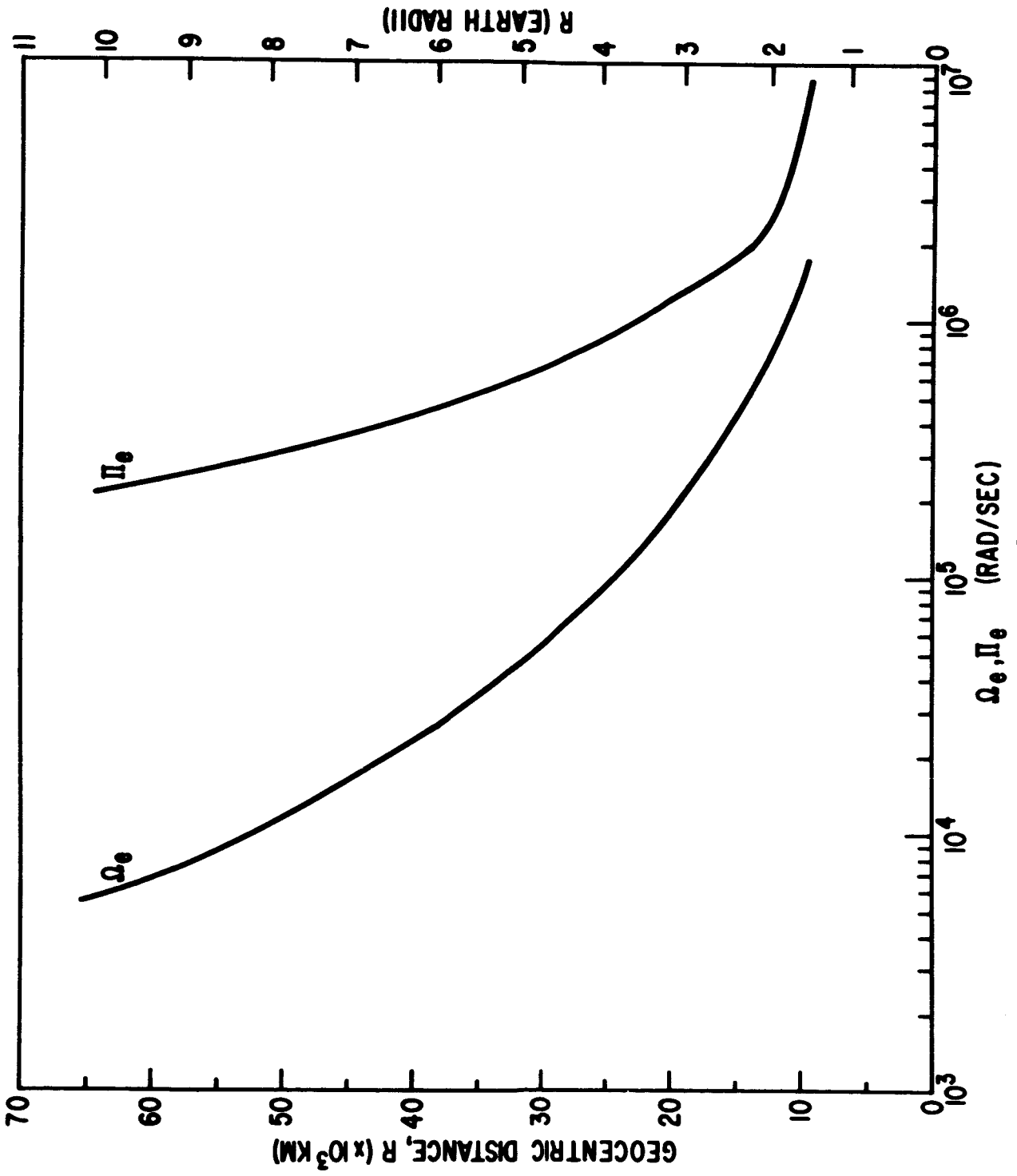


Figure 3.

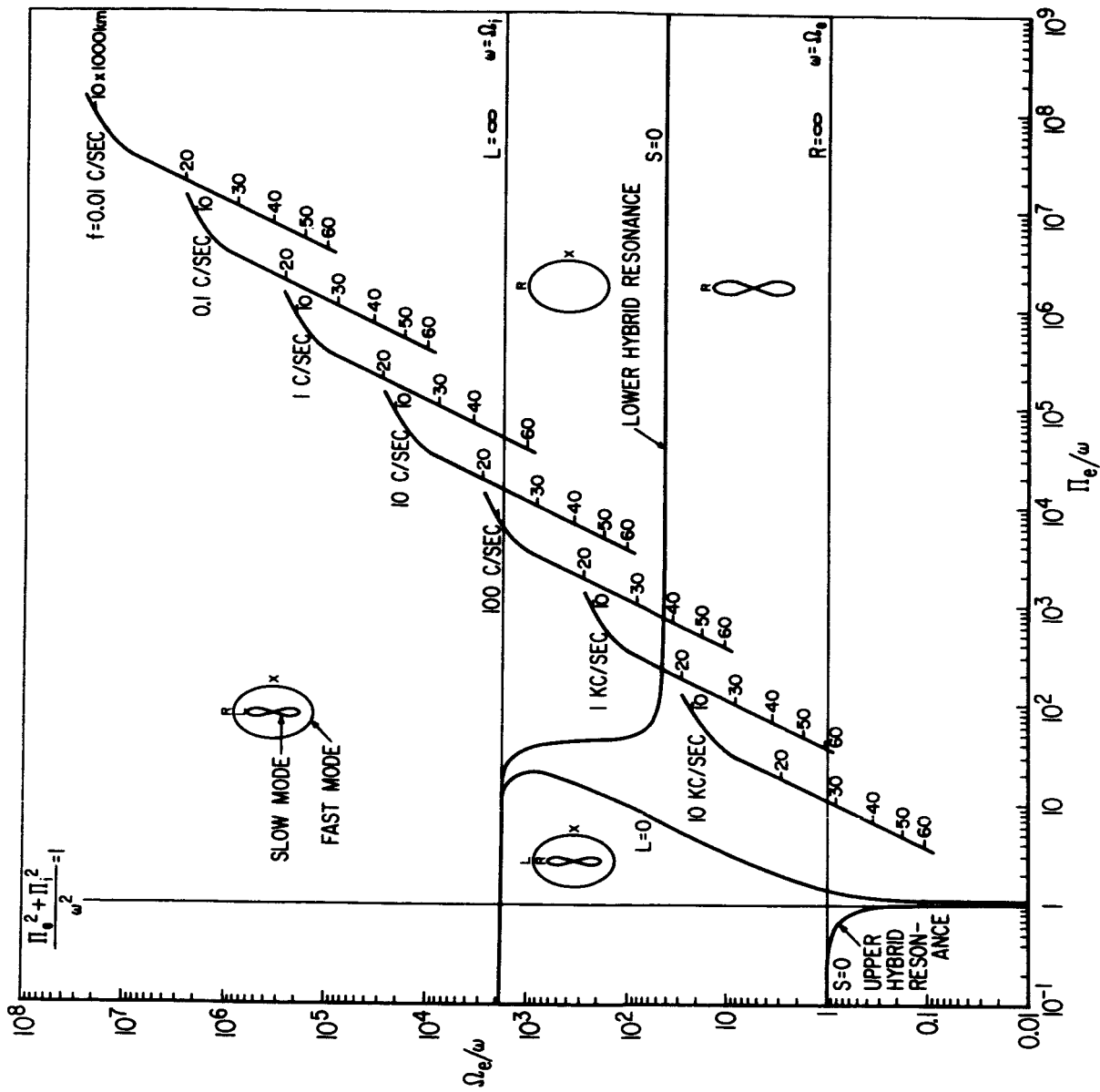


Figure 4.

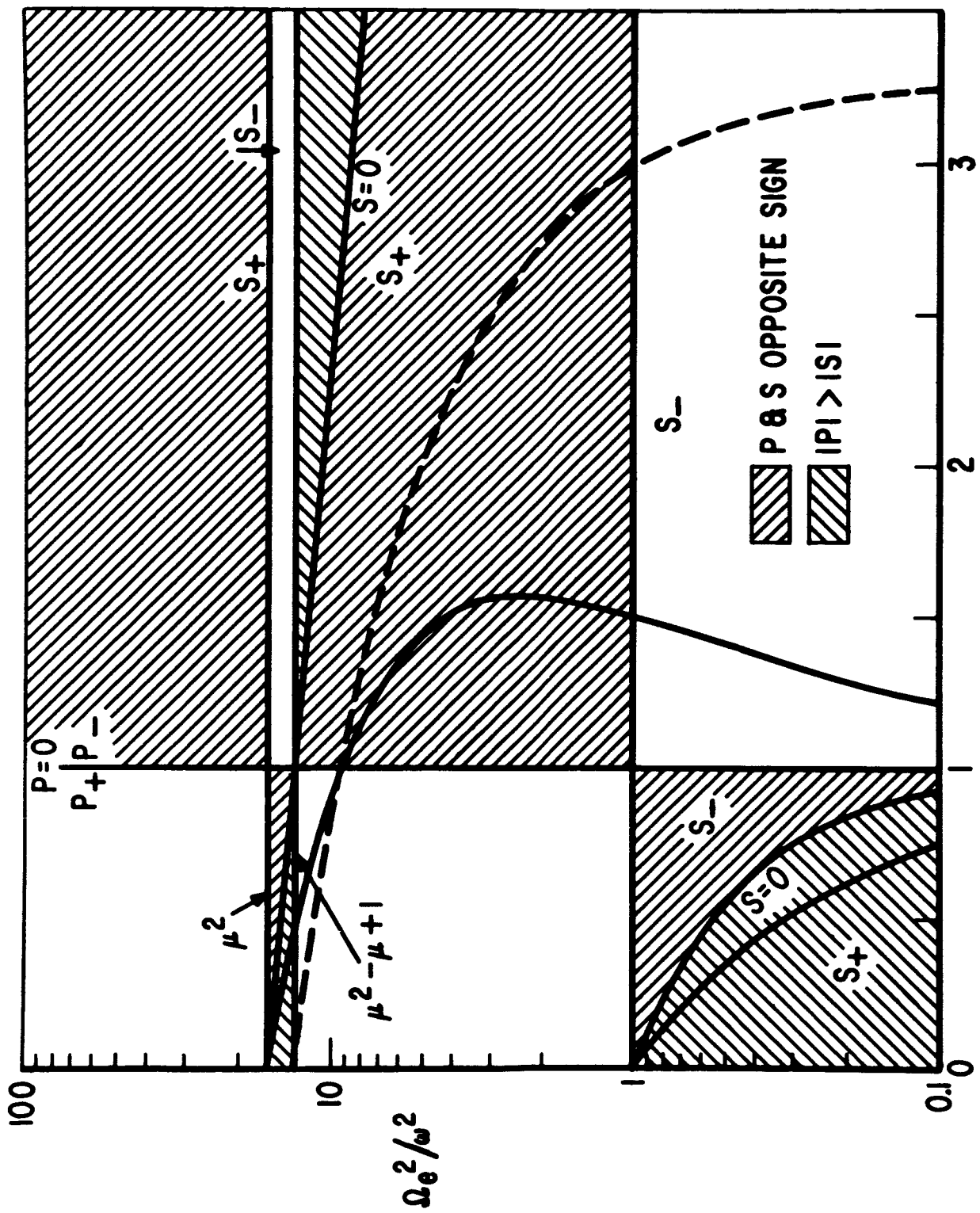


Figure 5.

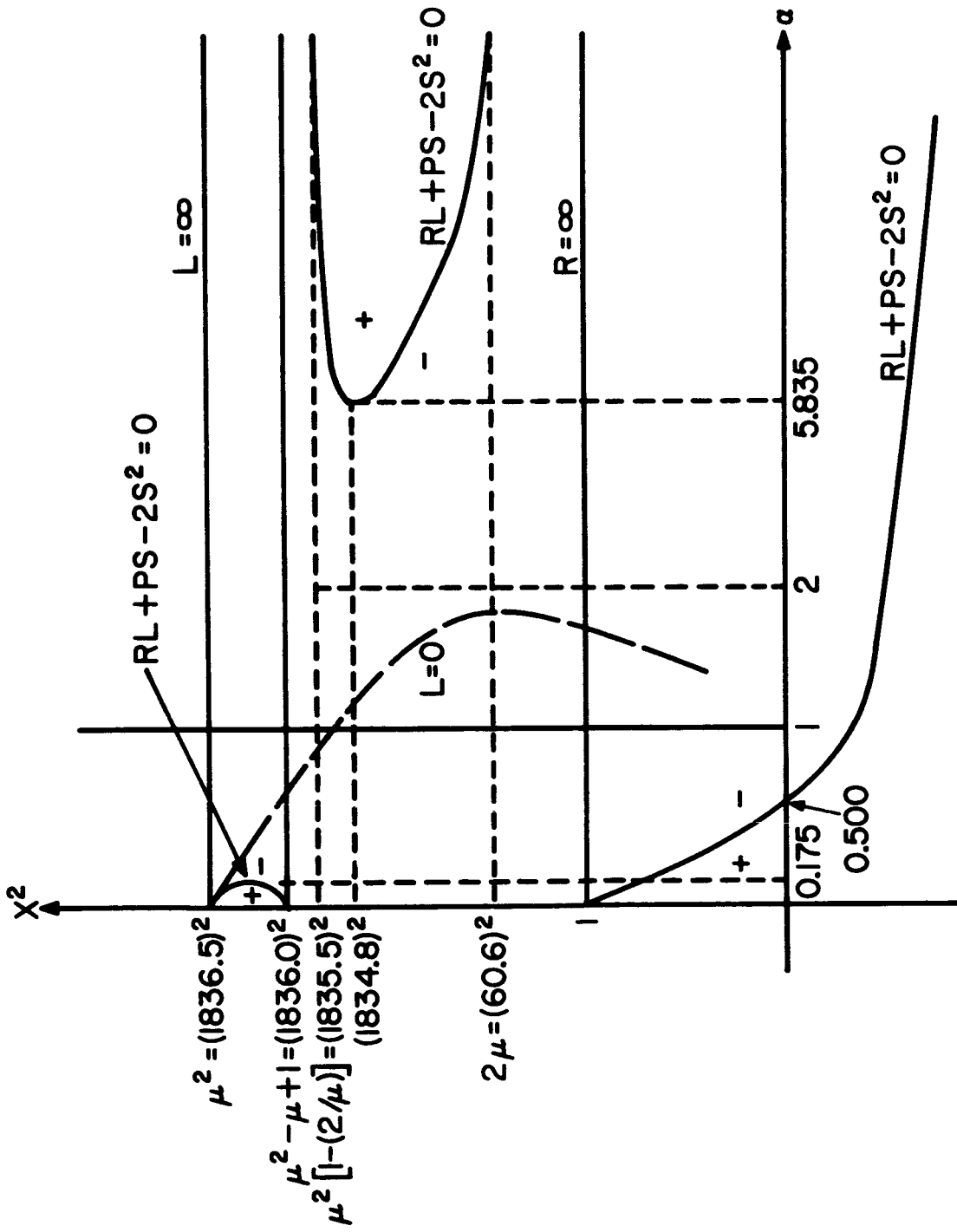


Figure 6.

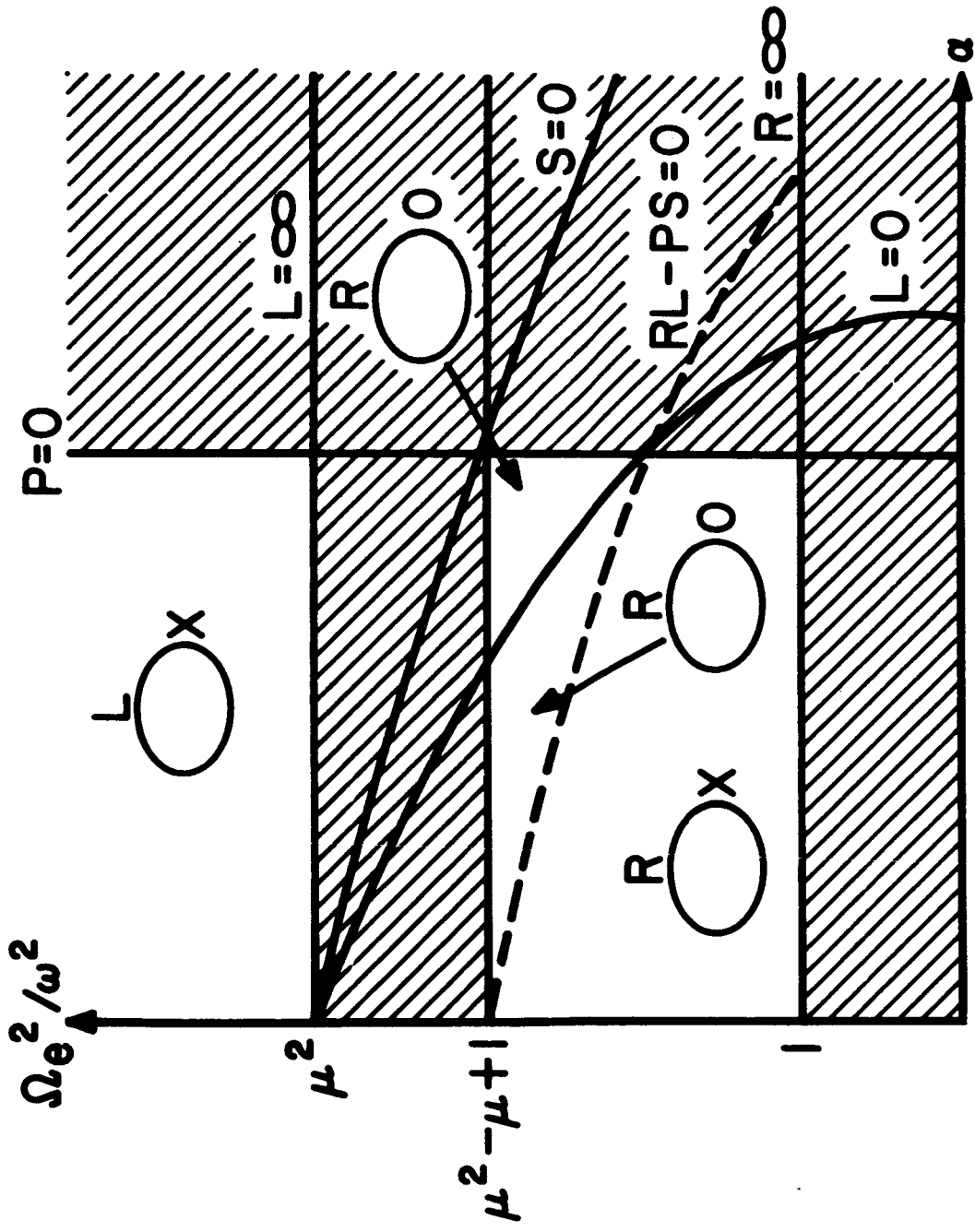


Figure 7.

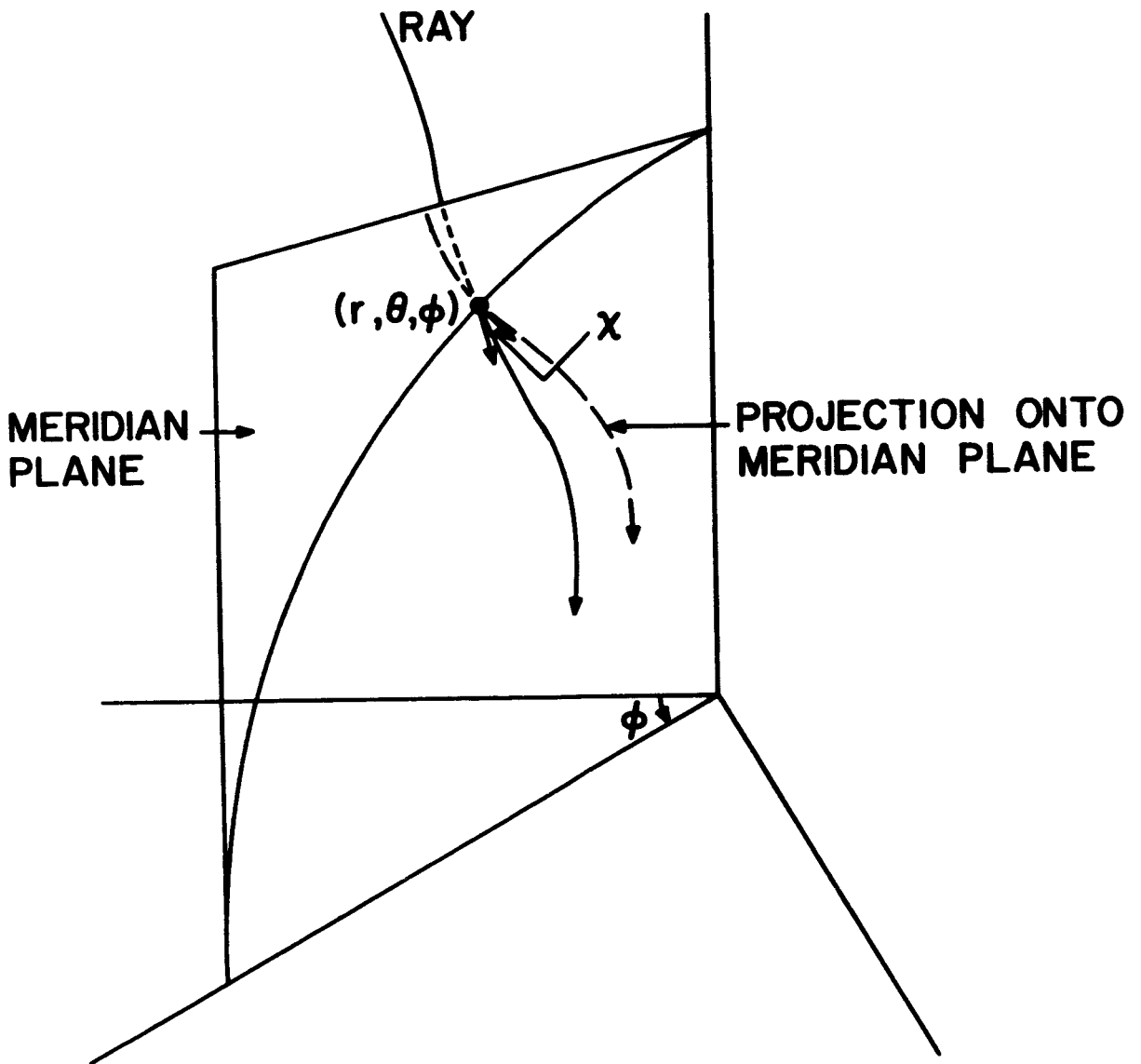


Figure 8.

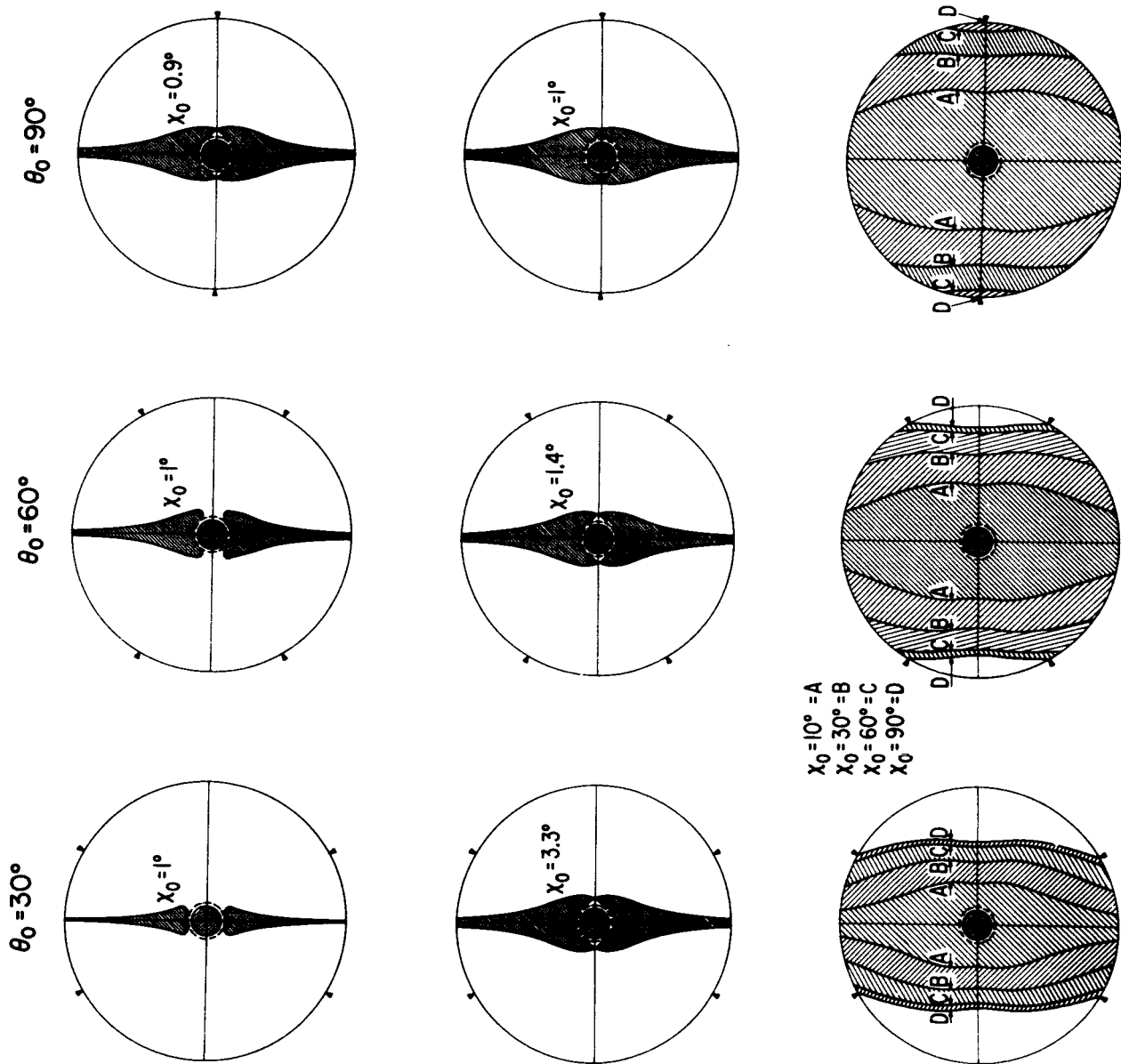


Figure 9.

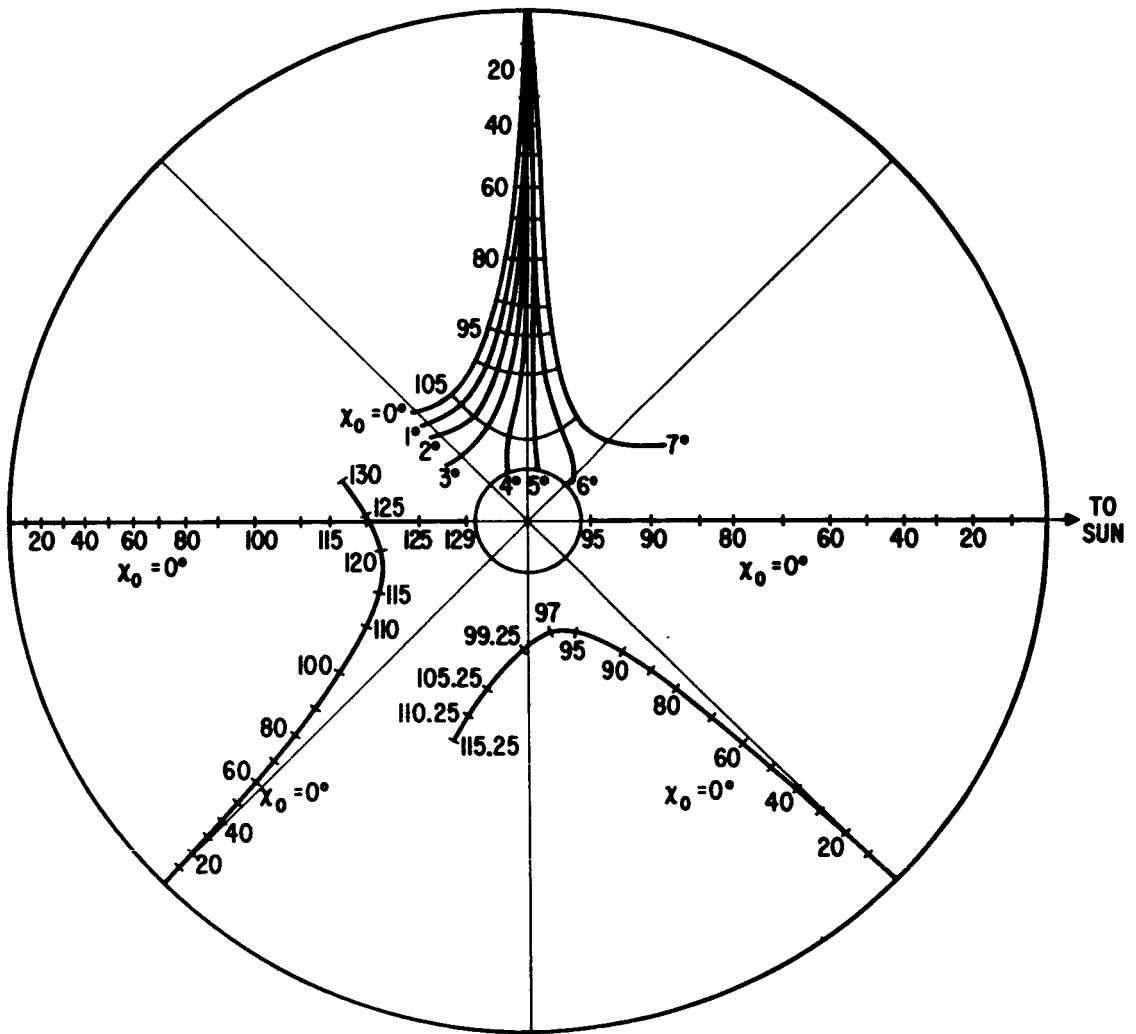


Figure 10.